

Temporal and Rate Coding for Discrete Event Sequences in the Hippocampus

Highlights

- CA1 neurons exhibited nonspatial event-specific elevated firing activities
- These “event cells” displayed transient theta phase precession at event onset
- Transient phase precession was followed by phase locking to early theta phases
- Theta sequences of CA1 neurons for event sequences had discrete representations

Authors

Satoshi Terada, Yoshio Sakurai,
Hiroyuki Nakahara,
Shigeyoshi Fujisawa

Correspondence

fujisawa@brain.riken.jp

In Brief

Terada et al. investigated the neuronal representations of nonspatial event sequences in the hippocampus and demonstrate that discrete event sequences are encoded by theta sequences of CA1 cell assemblies similar to space encoding.



Temporal and Rate Coding for Discrete Event Sequences in the Hippocampus

Satoshi Terada,¹ Yoshio Sakurai,² Hiroyuki Nakahara,³ and Shigeyoshi Fujisawa^{1,4,*}

¹Laboratory for Systems Neurophysiology, RIKEN Brain Science Institute, 2-1 Hirosawa, Wako, Saitama 351-0198, Japan

²Laboratory of Neural Information, Graduate School of Brain Science, Doshisha University, 1-3 Tatara Miyakodani, Kyotanabe, Kyoto 610-0394, Japan

³Laboratory for Integrated Theoretical Neuroscience, RIKEN Brain Science Institute, 2-1 Hirosawa, Wako, Saitama 351-0198, Japan

⁴Lead Contact

*Correspondence: fujisawa@brain.riken.jp

<http://dx.doi.org/10.1016/j.neuron.2017.05.024>

SUMMARY

Although the hippocampus is critical to episodic memory, neuronal representations supporting this role, especially relating to nonspatial information, remain elusive. Here, we investigated rate and temporal coding of hippocampal CA1 neurons in rats performing a cue-combination task that requires the integration of sequentially provided sound and odor cues. The majority of CA1 neurons displayed sensory cue-, combination-, or choice-specific (simply, “event”-specific) elevated discharge activities, which were sustained throughout the event period. These event cells underwent transient theta phase precession at event onset, followed by sustained phase locking to the early theta phases. As a result of this unique single neuron behavior, the theta sequences of CA1 cell assemblies of the event sequences had discrete representations. These results help to update the conceptual framework for space encoding toward a more general model of episodic event representations in the hippocampus.

INTRODUCTION

The hippocampus is fundamental for the neuronal encoding of episodic memory and spatial navigation (O’Keefe and Nadel, 1978; Tulving and Markowitsch, 1998; Burgess et al., 2002; Leutgeb et al., 2005), both of which consist of sequential representations of events or locations. These sequences involve both rate and temporal coding of information across the ensembles of active neurons. Rate coding takes the form of receptive fields of locations (i.e., place fields; O’Keefe and Dostrovsky, 1971), items (Wood et al., 1999; Quiroga et al., 2005), or time (Pastalkova et al., 2008; MacDonald et al., 2011; Kraus et al., 2013), while temporal coding can be seen in the phases of spike sequences on concurrent theta cycles, which shift as a function of distance relative to the center of the receptive field (i.e., phase precession; O’Keefe and Recce, 1993; Huxter et al., 2003; Buzsáki, 2002). With these two forms of coding, hippocampal cell

assemblies generate sequential structures across single theta cycles, termed theta sequences, which compressively represent sequences of past, current, and future positions (Skaggs et al., 1996; Dragoi and Buzsáki, 2006; Foster and Wilson, 2007). However, the mechanisms of theta sequence formation remain largely unknown (Mehta et al., 2002; Harvey et al., 2009; Royer et al., 2012; Wang et al., 2015; Feng et al., 2015; Middleton and McHugh, 2016).

Recent studies demonstrated that hippocampal theta sequences can reflect optic-flow signals (Terrazas et al., 2005; Cei et al., 2014), motion speed information (Geisler et al., 2007), and intentions of goal-directions (Wikenheiser and Redish, 2015; Pastalkova et al., 2008). Further, theta phase precession can be observed even in the absence of spatial movement (Harris et al., 2002; Pastalkova et al., 2008; Lenck-Santini et al., 2008; Takahashi et al., 2014). These observations indicate that theta sequences during spatial navigation might reflect the dynamic integration of multiple types of information including external cues, locomotion, and internal metrics of the animal (Feng et al., 2015). This predicts that information integration is essential for updating internal models of the current situation and reorganizing the temporal structure of cell assemblies within theta cycles (Tsodyks et al., 1996; Lisman, 2005; Hasselmo, 2005; McNaughton et al., 2006; Foster and Knierim, 2012). To test this hypothesis, it is crucial to control the timing of information updating. However, in spatial navigation or time perception tasks, this is difficult due to the continuous nature of space and time.

To address this, we developed a decision-making task that requires the integration of nonspatial information. In this task, the rat’s correct response is determined by a combination of two sensory cues (sound and odor). The key feature of this task is precise control of the timing of information updating by isolating two unique external inputs and sequencing the periods of the stimuli and choice actions. We found that many CA1 neurons showed stimulus-specific firing activities mostly sustained during the stimulus presentation period. Stimulus-specific cells demonstrated transient theta phase precession following stimulus onset but then became locked to early theta phases during the remainder of the stimulus presentation period. In consequence, the theta sequences of stimulus-specific cells had segmented and discrete representations. Our results indicate that information updating is essential for theta sequence

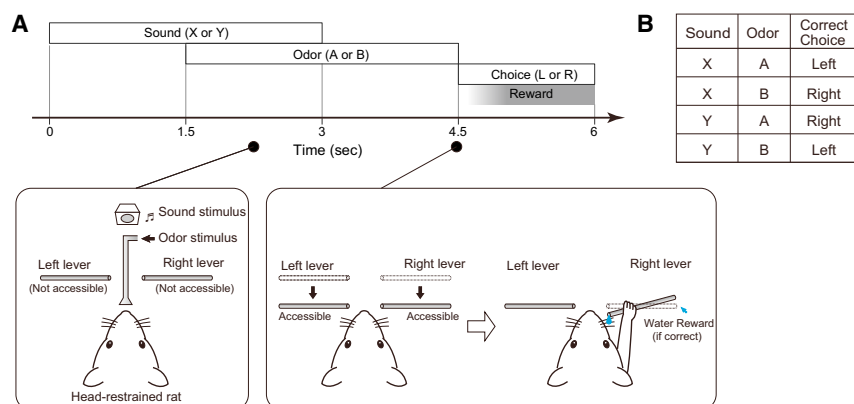


Figure 1. Schematic of a Cue-Combination Task

(A) A sound cue was presented during the period 0~3.0 s from trial onset, followed by an odor cue presented during the period 1.5~4.5 s. After the odor offset, the left and right levers moved to an accessible position, allowing the rat to perform a choice action. Water reward was provided from the tip of the lever following a correct choice.

(B) Table of correct choices and combination patterns of sound and odor cues.

formation in the hippocampus. We hypothesize that the hippocampus may employ a common computational framework for processing sequence information of both spatial navigation and episodic memory.

RESULTS

Rats were trained in a cue-combination decision-making task requiring the integration of sound and odor cues associated with left or right lever pulls under a head-restrained condition (Figure 1; Figure S1; Movie S1; STAR Methods). The correct choice (left or right lever) was determined by a combination pattern of sound (sound X or Y) and odor (odor A or B) cues in each trial. A sound cue was presented during the period of 0~3.0 s from trial onset, and an odor cue was presented during the period of 1.5~4.5 s. After offset of the odor cue, the left and right levers moved to an accessible position to allow the rat to make a choice action, that is, pulling the left or right lever to receive water drops provided from the tip of the lever (Isomura et al., 2009; Kimura et al., 2012) as a reward.

Rate Coding in CA1 for Integration of Nonspatial Information

We recorded multiple extracellular single units from hippocampal CA1 in four rats during the cue-combination task using high-density silicon probes (Table S1; STAR Methods; Fujisawa et al., 2008). Units were categorized as putative pyramidal neurons or interneurons based on the shapes of their waveforms and firing rates (Figure S1; Csicsvari et al., 1998). Units whose peak firing rate in the trials was greater than 8 Hz were used for further analysis ($n = 754$ units for putative pyramidal cells, $n = 504$ units for putative interneurons, in a total of 34 sessions).

To assess the stimulus- or choice-selective firing activities of CA1 single neurons in the task, we compared peri-stimulus time histograms (PSTHs) of the discharge activities of single neurons across different conditions during single sessions. First, we tested odor-cue-selective firing effects (Figures 2A and 2B). A large number of pyramidal neurons showed odor-selective elevated activity during the odor presentation period (1.5~4.5 s). Statistical tests with permutation methods (Figure S2; STAR Methods; Fujisawa et al., 2008) revealed that the firing rate of 51.6% of pyramidal cells had significant modulation

during the odor-presenting period (1.5~4.5 s) ($p < 0.05$; Figure 2B). Next, we estimated sound-cue-selective firing effects. Some neurons showed sound-selective activity with significant differences of PSTHs in the two conditions, but the total ratio of the significant cells was much lower than that of odor-cue-selective neurons (12.1% for sound presentation period 0~3sec; 4.5% for solely sound presentation period 0~1.5sec; Figures 2C and 2D). Finally, we assessed choice-selective firing effects and found that 74.5% of pyramidal cells had significantly modulated discharge rates (4.5~6 s) ($p < 0.05$; Figures 2E and 2F). Many interneurons also showed sound-, odor-, or choice-selective firing activities (Figure S3). These results indicate that CA1 neurons have stimulus-associated representations of sensory cues or choices in a nonspatial decision-making task.

To address whether CA1 neurons represented integrated information, in addition to simple sensory or motor information, we investigated the combination-selective firing activity in the task (Figures 3A and 3B; Figure S4). Comparisons of PSTHs of the single neurons across four combination conditions revealed that 20.3% of pyramidal neurons showed robust combination-selective sustained activities in the trials ($p < 0.05$; permutation tests were applied to compare most- versus 2nd-most-, most- versus 3rd-most-, and most- versus least-preferred combination trials. Bonferroni correction was applied for each comparison. See STAR Methods.). Note that the sustained activity of combination-selective neurons often outlasted not only the period of concurrent presentation of the sound and odor cues (1.5~3 s) but also the period of only odor cue presentation (3~4.5 s), indicating that combination-selective neurons did not merely represent multimodal (sound and odor) sensory stimuli but rather the conjunctive information of the two sensory cues associated with choice.

To assess the population activity of CA1 pyramidal cells during the task, auto-correlation of the population vectors in each combination condition was computed (Figure 3C; Figure S5; STAR Methods; Gothard et al., 1996). The population activities were clearly segmented in three periods, namely, solely sound-presenting period (0~1.5 s), odor-presenting period (1.5~4.5 s), and choice period (4.5~6 s), demonstrating that the stimulus- or choice-selective sustained activity in these periods is supported on the population level. To assess similarities and differences of population activities in different conditions, cross-correlations of

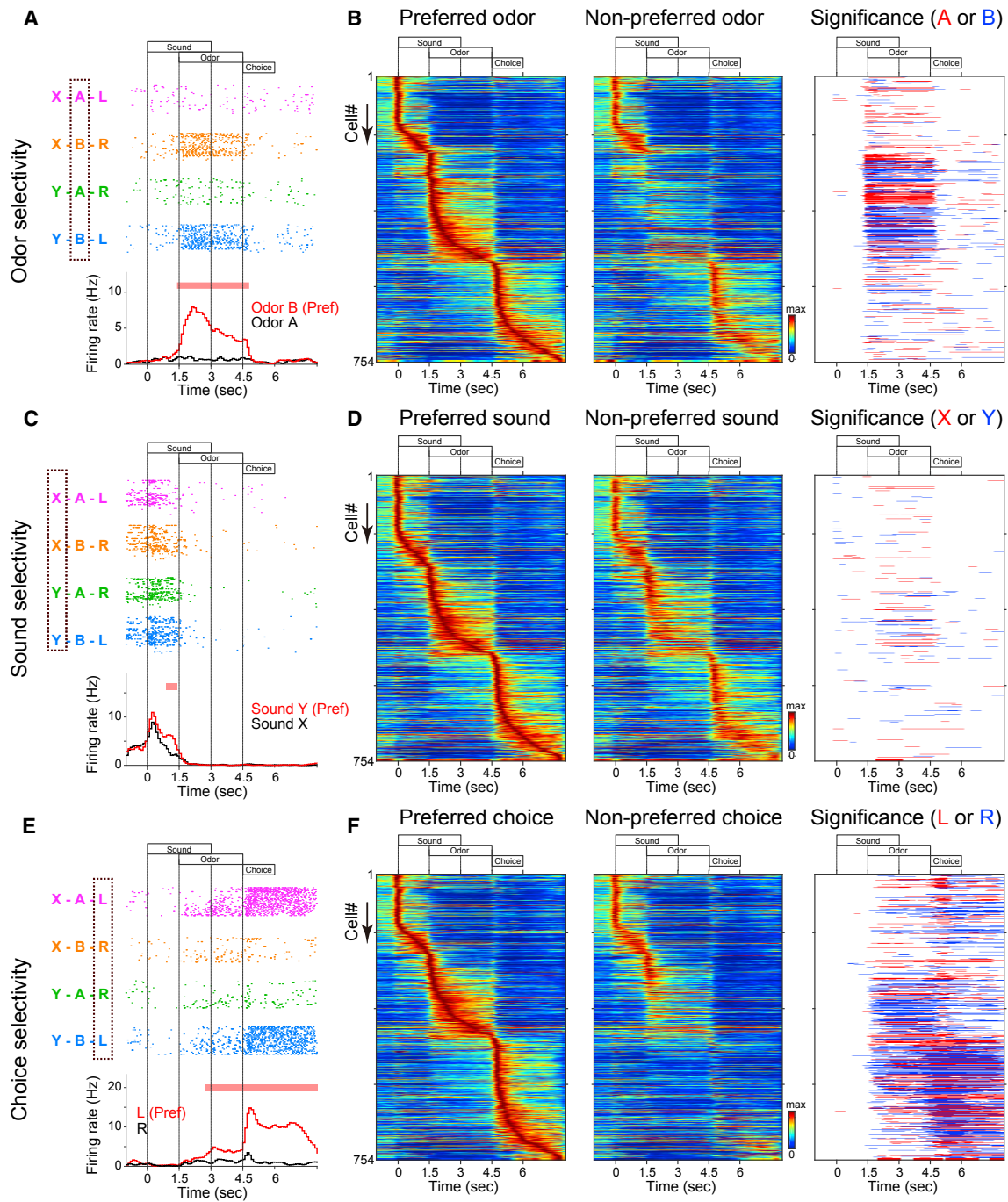


Figure 2. Odor-, Sound-, or Choice-Selective Firing Activity of Single CA1 Neurons

(A) Firing patterns of a representative odor-selective neuron. Top, raster plots of each combination condition. Bottom, PSTHs of odor A (black; combinations X-A-L and Y-A-R) and odor B (red; X-B-R and Y-B-L). Red line above PSTHs shows a segment with significantly higher firing rates during odor-B trials ($p < 0.05$; permutation test; see STAR Methods; Figure S2).

(B) Firing patterns of CA1 pyramidal neurons during preferred (first column) and nonpreferred (second column) odor trials ($n = 754$ units; the same set of neurons was used in D and F). Each row represents the PSTH of a single neuron. Color scale represents firing rate of each neuron (red represents max firing rate of each neuron and blue represents 0 Hz). Neurons were ordered by the time of their peak firing rates. Third column shows segments with significantly higher discharge rates in odor-A (red) or odor-B (blue) trials.

(C) Firing patterns of a representative sound-selective neuron.

(legend continued on next page)

the population vectors across different combination conditions were also computed (Figure 3C; Figure S5C). In the odor-presenting period (1.5~4.5 s), the population activities of each combination condition were similar to those of same-odor combination conditions (“same-odor counterparts”) (Figure S5D). In the choice period (4.5~6 s), population activities were similar to those of same-choice conditions (“same-choice counterparts”) (Figure S5E). Otherwise, auto-correlation was significantly higher than cross-correlations (Figures S5D and S5E).

We also compared the neuronal firing patterns between correct and error trials (Figure 3D; Figure S5). Cross-correlations of population vectors between correct and error trials in same or different conditions were always lower than auto-correlations of population vectors in correct trials (Figure 3D; Figures S5D and S5E), though the overall mean firing rates of neurons were not different (Figure S5B).

Transient Phase Precession Followed by Phase Locking to Early Theta Phase

During the task, the simultaneously recorded local field potential (LFP) was dominated by a robust theta frequency (5–12 Hz) oscillation (Figure S6A). The spiking of 91.4% of pyramidal and 99.8% of interneurons was significantly phase-modulated by the theta oscillation ($p < 0.01$, Rayleigh test; Figure S6B). We analyzed the phase-time relationships of single neurons to check for the presence of theta phase precession as a function of time from trial onset. With our criteria (Figure S6C; STAR Methods), 62.6% of pyramidal neurons demonstrated phase precession in at least one of the combination conditions during the task trials (Figure S6D).

Next, we assessed the relationship of stimulus- or choice-selective firing rate increases with theta phase precession. We first compared phase-time relationships in different odor conditions in odor-selective neurons ($n = 152$ units) and observed robust theta phase precession in the preferred-odor trials, but not in the nonpreferred-odor trials (Figures 4A and 4B; Figures S6E and S7A). Permutation tests were applied to determine the significant differences of the theta phases between preferred- and nonpreferred-odor trials and revealed that 91.4% of the odor-selective cells showed significant differences in the theta phase shift between preferred- and nonpreferred-odor trials during the odor-presenting period (1.5~4.5 s) (Figure 4B). Importantly, following this transient phase precession (Figure S6H), these neurons with elevated activity became locked to descending phases (0° – 180°) of theta in the preferred-odor trials (Figure S7A). We ruled out the possibility that the absence of phase precession in nonpreferred trials was because theta phase precession could not be detected due to lower firing rates, by using a random resampling method (Figure S8). We next analyzed the phase-time relationships in choice-selective neurons ($n = 222$ units) during the choice period (4.5~6 s) and found that 85.1% of neurons showed a significant phase shift in preferred-choice

trials compared to nonpreferred-choice ones (Figures 4C and 4D; Figures S6F and S7B). We also tested combination-selective neurons ($n = 72$ units) during odor-presenting periods and found that 56.9% of neurons had a significant phase shift between most-preferred combination trials and other combination trials (Figures 4E and 4F; Figures S6G and S7C).

In contrast, interneurons did not show phase precession during the trials. However, the stimulus-, choice-, or combination-selective interneurons showed a slight but significant phase shift in preferred trials compared to nonpreferred trials (Figure S9).

Theta Sequence Generation in the Cue-Combination Task

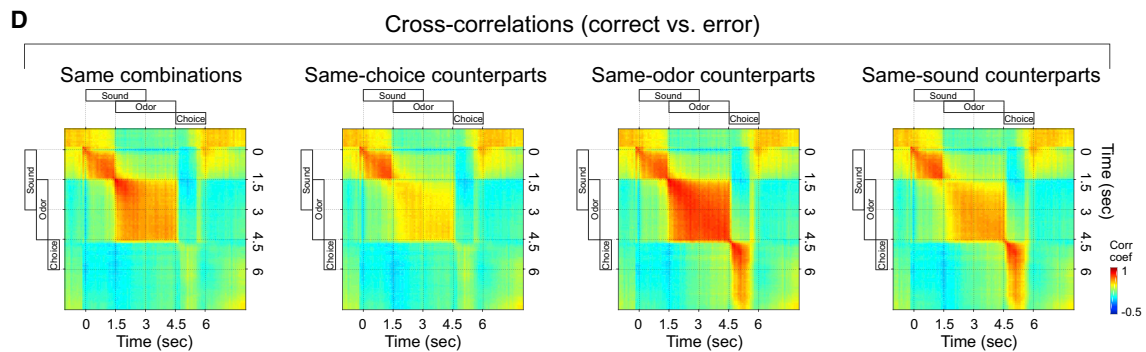
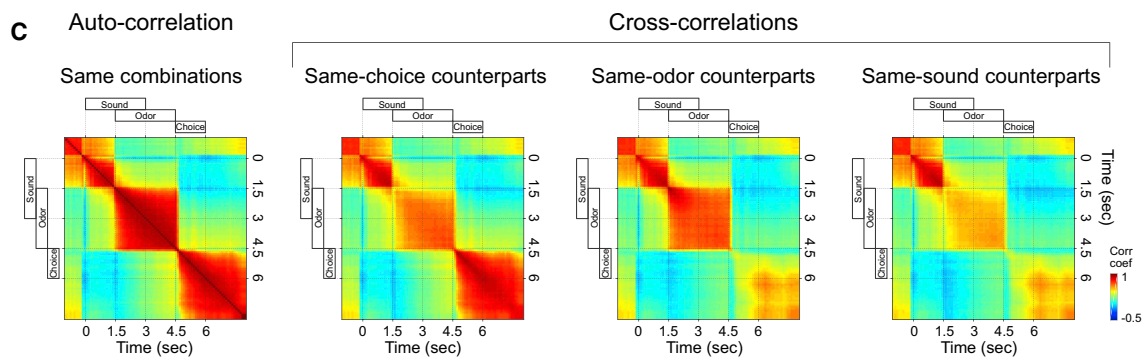
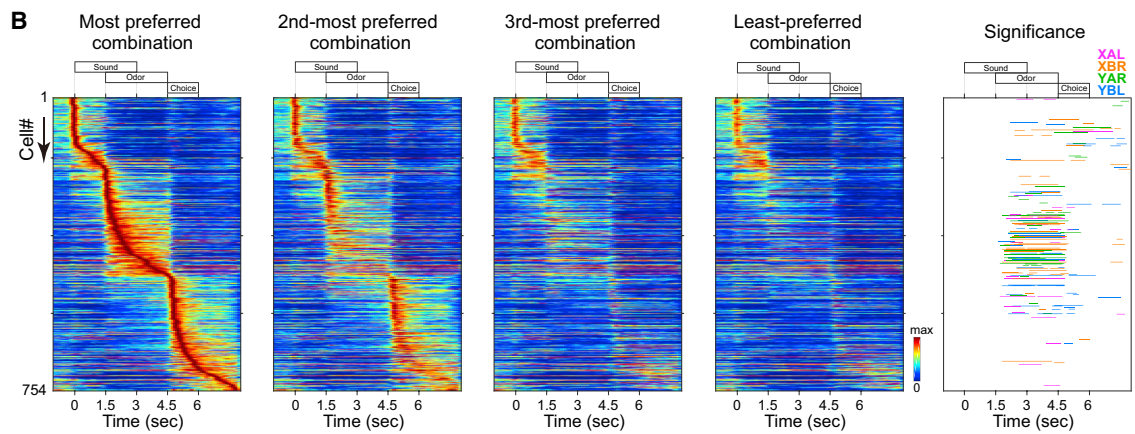
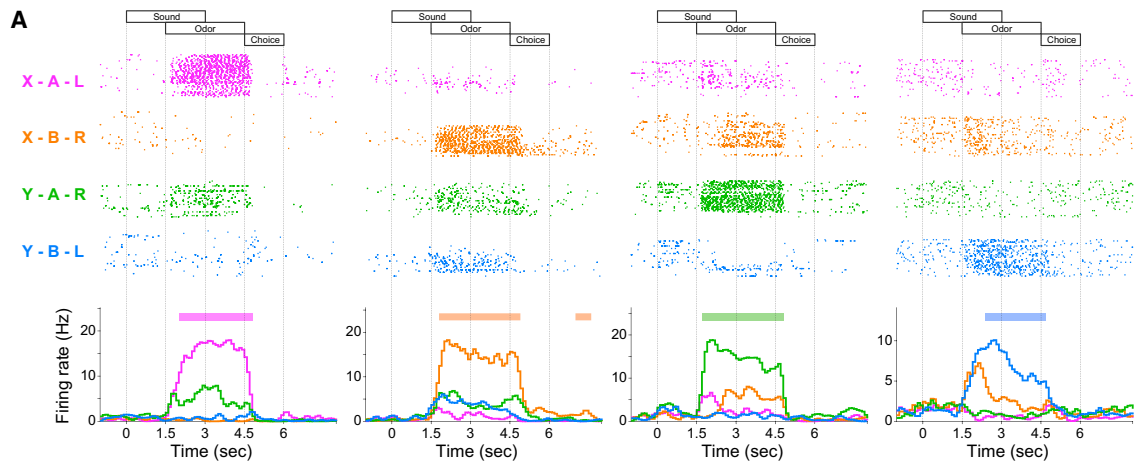
Theta phase precession of single neurons does not always guarantee the concurrent presence of theta sequences of cell assemblies (Feng et al., 2015; Middleton and McHugh, 2016). Thus, to address whether theta sequences were present in the task, we investigated the temporal structure of spike sequences in single theta cycles. First, pairwise analysis of theta sequences in the trials was performed (Dragoi and Buzsáki, 2006). If theta sequence is present in spatial navigation, the distance of place fields of a neuronal pair should be reflected in the distance of spiking phases of them in single theta cycles, which can be estimated by cross-correlation analysis in single trials (Dragoi and Buzsáki, 2006). We applied this pairwise analysis to assess whether the difference of PSTH peak times of a neuronal pair was reflected in the difference of spiking theta phases (STAR Methods). Figure 5A shows three example neurons simultaneously recorded in a single session. CCGs of spike times of the pair neurons during the trials revealed strong theta modulation on the interactions of these units. Moreover, the shifts of peak times of CCGs were correlated with the differences of the peak times of the PSTHs of the pairs (Figure 5B), indicating that the sequence activities of firing rates of the neurons were robustly compressed in single theta cycles. Group analysis of neuronal pairs revealed that the CCG peak shifts had a significant positive correlation with peak-time differences of firing rates of the pairs (Figure 5C; $n = 4585$ pairs; coefficient of determination $R^2 = 0.18$; $p < 0.001$; see STAR Methods), suggesting the presence of theta sequences in the cue-combination task.

We also investigated the theta sequences of cell assemblies in the trials using a Bayesian decoding technique (Zhang et al., 1998; Davidson et al., 2009; Feng et al., 2015). The probability densities of time information were reconstructed from simultaneously recorded pyramidal cell activities at every 5-ms time step in each trial (Figure S10A; STAR Methods). Figure 6A represents the reconstructed time information at each time point in a single example trial. Then, we aligned the reconstructed time information with concurrent theta phases (Figure S10A). The probability densities of the reconstructed time at each theta phase (Figures 6B and 6C) demonstrated robust theta sequence formation. On descending phases of theta (0° – 180°), the decoded

(D) Firing patterns of CA1 pyramidal neurons during preferred (first column) and nonpreferred (second column) sound trials. Third column shows segments with significantly higher discharge rates in sound-X (red) or sound-Y (blue) trials.

(E) Firing patterns of a representative choice-selective neuron.

(F) Firing patterns of CA1 pyramidal neurons during preferred (first column) and nonpreferred (second column) choice trials. Third column shows segments with significantly higher discharge rates in choice-L (red) or choice-R (blue) trials.



(legend on next page)

probability densities of time reflected the period during which the spikes were sampled. On the other hand, on ascending phases of theta (180° – 360°), decoded probability densities of time reflected future task sequences, in the sampling period of 0 to 4.5 s. A crucial difference between these sequences and those observed during spatial navigation (e.g., Feng et al., 2015) is that our sequences are not continuous but rather discrete and segmented.

We next examined whether the observed theta sequences included information reflecting the current combination conditions and future choices in addition to the time from trial onsets. The probability densities of time and combination, i.e., $P(\text{time, combination} | \text{spikes})$, were estimated from spikes (sampled in the time period 3~4.5 s) recorded during correctly answered trials (Figure 6D; Figure S10B; STAR Methods). Information of the combination conditions for current trials was correctly represented on the descending phases of theta (Figure 6E), while information of future choice directions was represented on the ascending phases (Figure 6F). On the other hand, the decoding results of probability densities of time and combination from spikes in error trials showed that wrong combinations were represented on descending phases (Figure 6E) and that the wrong choices were represented on ascending phases (Figure 6F). Note that the probability densities in the error trials on the ascending phases were highest in same-odor counterpart combinations (i.e., odor was correctly decoded but sound was incorrect; Figure 6E), implying that the auditory cue was either miscoded or ignored in the error trials (Hampson et al., 2004). These results indicate that the information sequences representing both current combination conditions and future choice actions were robustly compressed within theta cycles.

Changing the Temporal Order of Cue Stimuli

Finally, in order to investigate whether theta sequences reflect changes in the order of the event sequences, we switched the presentation order of sound and odor stimulations without changing the combination-choice contingency (Figure 7A; Table S1). In the new stimulus order sessions, an odor cue was presented during the period of 0~3.0 s from trial onset, and a sound cue was presented during the period of 1.5~4.5 s. In the first day of this switch, the task performance of the rats was decreased to around 50% (Figure S11A), and the neuronal ensemble activities were partially “remapped” (Figures S11B–S11F). However, after a few days of training, the rats adapted to the new presentation order and performed the task well (Figure S11A).

Figure 7 shows the rate and temporal coding of odor-, choice-, and combination-selective neurons in the sessions with the new stimulus order (Table S1). Here, the odor-selective neurons had phase precession around the odor cue onsets (Figures 7B and 7C). On the other hand, the combination-selective neurons exhibited phase precession around the onset of simultaneous presentations of odor and sound (Figures 7F and 7G), identical to what we observed under the initial task conditions (Figure 4). The choice-selective neurons also showed features similar to those recorded prior to the order switching (Figures 7D and 7E). Pairwise analysis of theta sequences revealed that correlation of the peak-time shifts of CCGs and peak-time differences of the PSTHs of neuronal pairs was also preserved after order switching (Figure 7H; $n = 994$ pairs; $R^2 = 0.13$; $p < 0.001$). A Bayesian decoding analysis also demonstrated that the theta sequences included the correct combination and choice information in correct trials (Figures 7I and 7J). Theta sequences in error trials included same-odor counterpart combination and wrong choice information (Figures 7I and 7J), as similar to those before switching (Figures 6E and 6F). These results indicate that theta sequences can be flexibly reorganized to reflect the order of event sequences.

DISCUSSION

In this study, we demonstrate that CA1 pyramidal cells employ both rate and temporal coding to represent discrete, nonspatial event sequences. The cue-combination task under head-restrained conditions enabled us to control the onset and offset of sound and odor cues and the timing of information integration. We found that a large number of CA1 neurons showed cue-, combination-, or choice-specific (in short, “event”-specific) sustained activity during trials, which accompanied transient theta phase precession followed by sustained phase locking to early theta phases during specific events. As a result, the theta oscillation temporally organized CA1 cell assemblies into discrete event sequences (Figure 8).

Hippocampal Representations for Spatial and Nonspatial Information

The cognitive map theory states that the hippocampus organizes internal maps representing the external world (Tolman, 1948; O’Keefe and Nadel, 1978). The majority of studies focused on place cells (O’Keefe and Dostrovsky, 1971; Wills et al., 2005; Leutgeb et al., 2005; McNaughton et al., 2006) and their ensemble dynamics (O’Keefe and Recce, 1993; Skaggs et al.,

Figure 3. Combination-Selective Firing Activity of Single CA1 Neurons

(A) Firing patterns of four representative combination-selective neurons. Lines above PSTHs represent segments with significantly higher firing rates during most-preferred combination trials ($p < 0.05$; permutation tests were applied to compare most- versus 2nd-most-, most- versus 3rd-most-, and most versus least-preferred combination trials. Bonferroni correction was applied for each comparison. Line colors represent most-preferred combination.).
 (B) Firing patterns of pyramidal neurons in most-preferred, 2nd-most-preferred, 3rd-most-preferred, and least-preferred (first to fourth column, respectively) combination trials ($n = 754$ units; the same set of neurons as shown in Figure 2B were used). Neurons were ordered by the time of their peak firing rates in most-preferred combinations. Fifth column shows segments with significantly higher discharge rates in most-preferred combination trials.
 (C) Auto-correlation and cross-correlations of population vector matrices of combination conditions. The procedures of the analysis and meanings of “same combinations,” “same-choice counterparts,” “same-odor counterparts,” and “same-sound counterparts” are described in Figure S5 and STAR Methods.
 (D) Cross-correlations of population vector matrices between correct and error trials. x axis represents the time for error trials and y axis for correct trials. See also Figure S5.

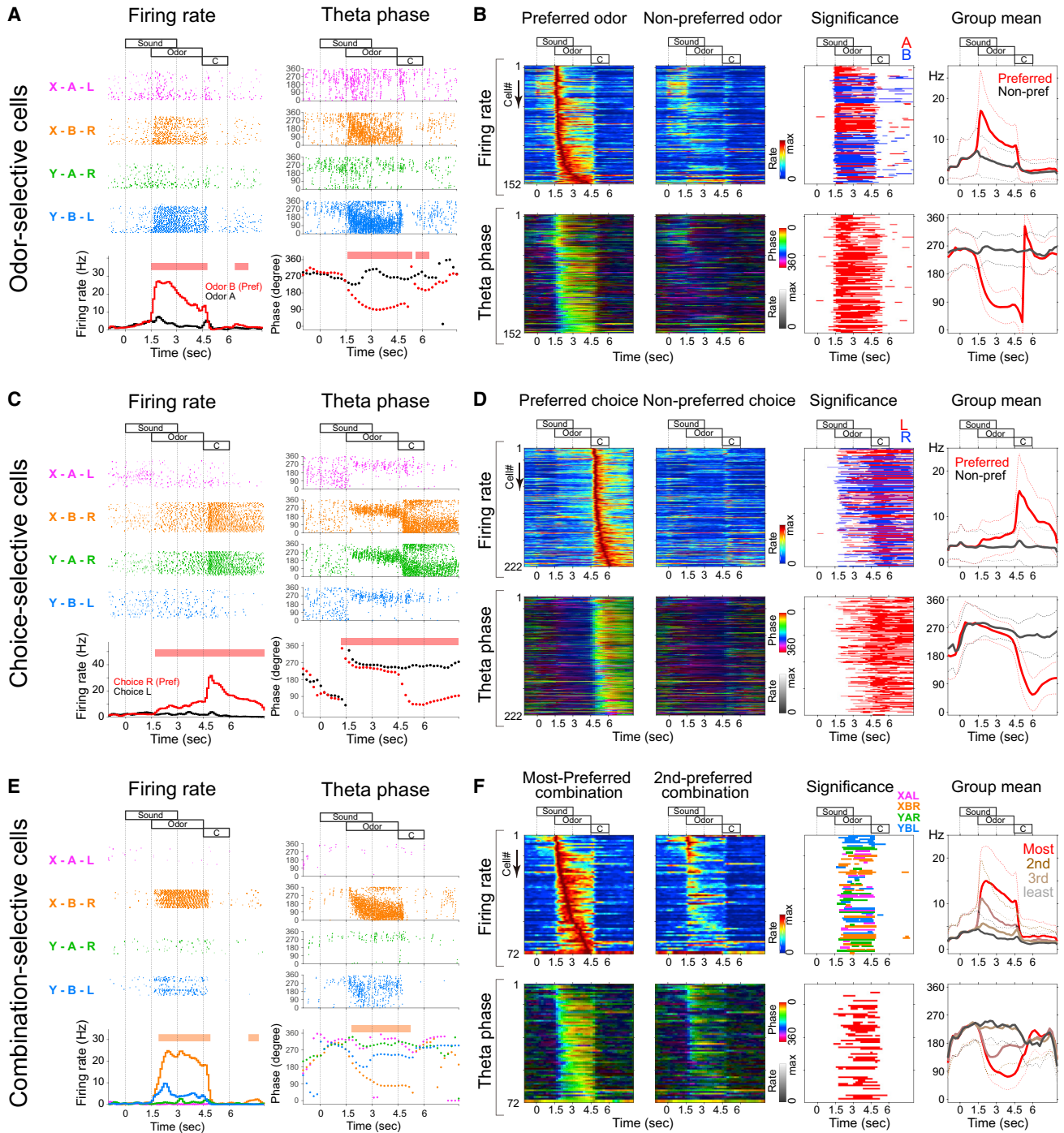


Figure 4. Temporal and Rate Coding of Single Pyramidal Neurons during the Cue-Combination Task

(A) Firing rates and theta phases of a representative odor-selective neuron. Left, raster plots and PSTHs. Right top, theta phase plots as a function of time from stimulus onset. Each dot represents an action potential. Right bottom, mean theta phases as a function of time during odor-A (black) and odor-B (red; preferred) trials. Red lines above PSTHs and phase plots show segments with significantly higher firing rates and with significant phase differences during preferred trials, respectively ($p < 0.05$; permutation test; same for (C)).

(B) Firing rates and theta phases of all odor-selective neurons. Odor-selective neurons were defined as neurons that had significant rate differences between Odor-A and -B trials in odor-presenting periods ($n = 152$ units). Top, firing rates of odor-selective neurons during preferred- and nonpreferred-odor trials. Color scale represents firing rate of each neuron (red represents max firing rate of each neuron and blue represents 0 Hz). Neurons were ordered by the time of their peak firing rates. Third column shows segments with significantly higher discharge rates in odor-A (red) or odor-B (blue) trials ($p < 0.05$; permutation test). Right column shows mean firing rates (thick lines) \pm SD (dotted lines). Bottom, theta phases as a function of time during preferred- and nonpreferred-odor trials. Hue

(legend continued on next page)

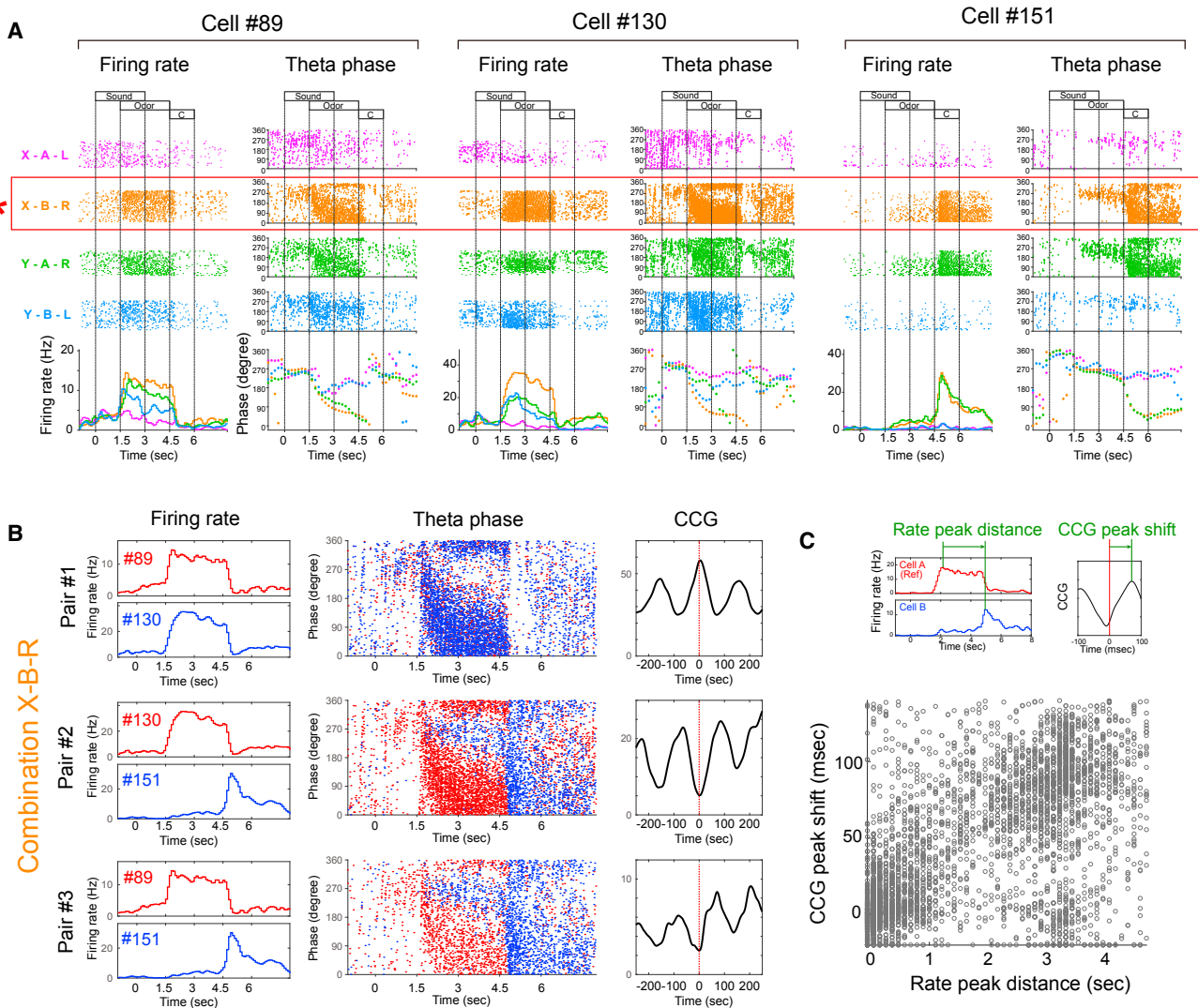


Figure 5. Pairwise Analysis of Temporal Compression of Spike Sequences in Single Theta Cycles

(A) Firing rates and theta phases of three representative neurons recorded simultaneously.

(B) Cross-correlations (right column) of the three pairs of neurons during the combination X-B-R trials (indicated with the asterisk in A). Left column, PSTHs of the neurons. Center column, theta phase plots of the neurons as a function of time from stimulus onset. Each dot represents an action potential.

(C) Pairwise analysis of temporal compression of spike sequences in single theta cycles. Each dot represents a single neuronal pair in a single combination. x axis shows peak distances of firing rates, and y axis shows peak shifts of CCGs (insets). Reference neurons for CCG were the ones whose PSTH peaks occurred earlier than the others. The criteria for pair selection are described in [STAR Methods](#) ($n = 4585$ pairs; $R^2 = 0.18$; $p < 0.001$).

1996; Dragoi and Buzsáki, 2006; Foster and Wilson, 2006; Pfeiffer and Foster, 2013) illustrate this theory in the context of spatial navigation. However, the hippocampus is also critical

for the memory of nonspatial event sequences in humans (Squire and Zola-Morgan, 1991; Aggleton and Brown 1999; O'Reilly and Rudy, 2001) and animals (Bunsey and Eichenbaum, 1996; Dusek

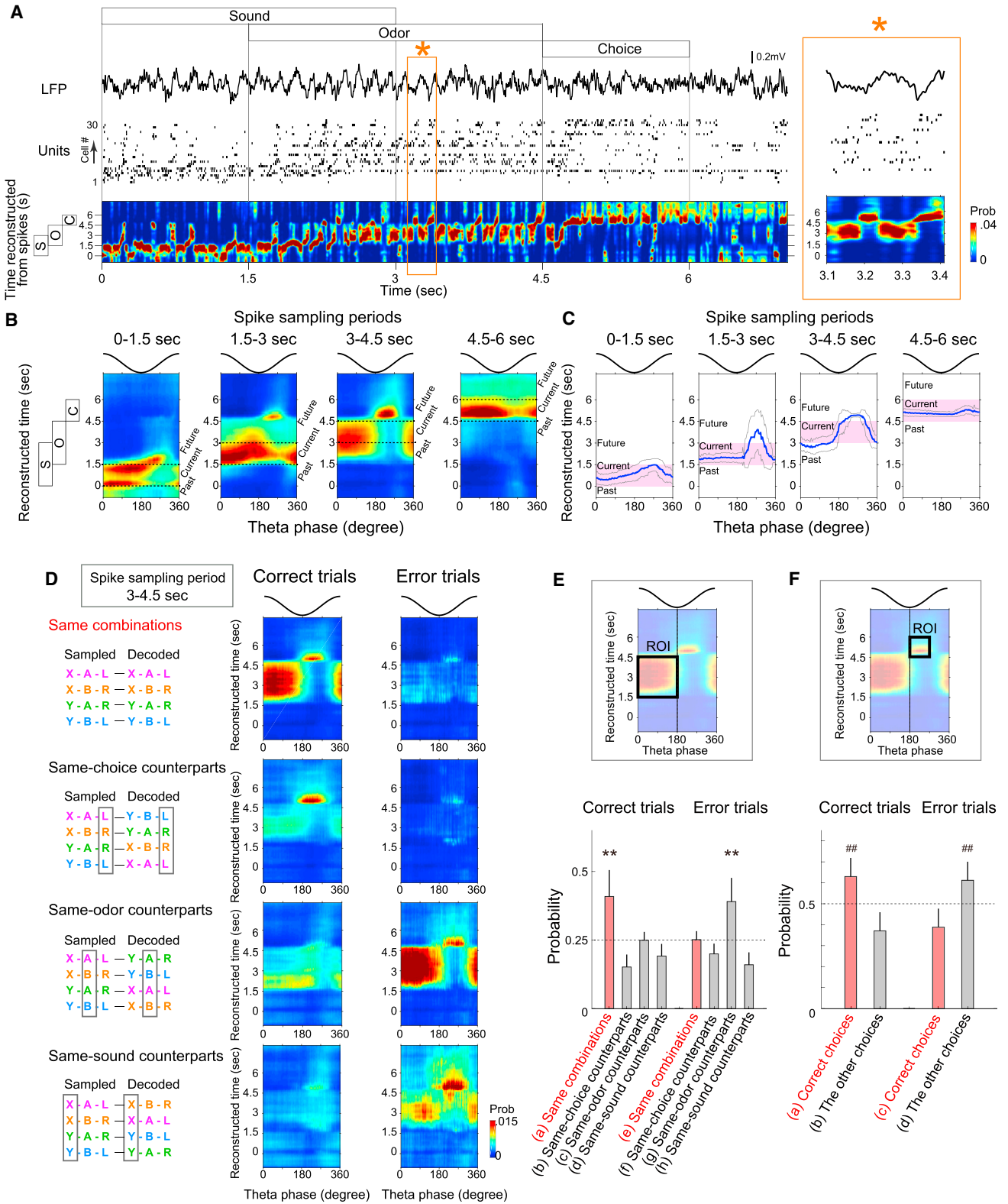
represents theta phases (0° – 360°), and brightness represents normalized firing rates in each neuron. Third column shows segments with significantly different phases in different odor trials ($p < 0.05$; permutation test; see [STAR Methods](#)). Right column shows mean phases \pm SD.

(C) Firing rates and theta phases of a representative choice-selective neuron.

(D) Firing rates and theta phases of all choice-selective neurons. Choice-selective neurons were defined as neurons that had significant rate differences between choice-L and -R trials in choice periods ($n = 222$ units).

(E) Firing rates and theta phases of a representative combination-selective neuron. Lines above PSTHs and phase plots represent segments with significantly higher firing rates and with significant phase differences during most-preferred combination trials, respectively ($p < 0.05$; see [STAR Methods](#)).

(F) Firing rates and theta phases of all combination-selective neurons. Combination-selective neurons were defined as neurons that had significantly higher rates in specific combinations in sound and odor presentation periods ($n = 72$ units).



(legend on next page)

and Eichenbaum, 1997; Agster et al., 2002; Fortin et al., 2002); thus, this theory has been extended to embrace map-like representations of nonspatial information, including events and episodes (O'Keefe and Nadel, 1978; Eichenbaum, 2004; Buzsáki and Moser, 2013). Physiological data have revealed that hippocampal single neurons can represent event components such as olfactory (Eichenbaum et al., 1987; Wiener et al., 1989), auditory (Sakurai, 1990, 1996), visual (Sakurai, 1996), and item (Wood et al., 1999; Quiroga et al., 2005) information. Moreover, hippocampal neurons also display conjunctive representations of event components, for example, item and space (Komorowski et al., 2009; McKenzie et al., 2014; Wirth et al., 2003), item and time (Naya and Suzuki, 2011), and item and sequence (Manns et al., 2007a; Allen et al., 2016; Paz et al., 2010). Here, we demonstrate the conjunctive representations of purely nonspatial information in CA1. The key feature of our task is that the correct choice is determined by a combination of two cues and cannot be determined by either cue alone (Watanabe, 1986a, 1986b; Sutherland and Rudy, 1989). Thus, a simple direct association of either cue with the choice is not sufficient, but rather association with the cue combination is necessary. Many pyramidal neurons showed representations of single cue combinations, which can be dissociated from either sensory cue or choice action alone. These combinatorial responses are not simple representations of multimodal sensory stimuli, since combination-specific neurons often showed sustained activity not only during the selective period of simultaneous representation of sound and odor cues (1.5–3 s) but also during the periods of presentations of only odor cues (3–4.5 s) (Figures 3A and 3B). Thus, our results demonstrate that CA1 neurons represent the conjunctive associations of multimodal sensory signals that link cue and choice information.

Together with previous studies, our current results support the idea that the role of the hippocampus is to organize “relational networks” of event components to subservise episodic memory (Eichenbaum, 2004; Eichenbaum and Cohen, 2014). This concept is consistent with the hippocampal cognitive map hypothesis for spatial navigation, as routes in space can be considered as relational networks of positional information (Eichenbaum and Cohen, 2014).

The next question we addressed is how temporal order of these spatial or nonspatial event components is physiologi-

cally represented across the neuronal ensembles. During navigation, spatial order is encoded by the theta phase information of spiking activities. Place cell assemblies generate theta sequences, which compressively represent sequences of past, current, and future positions within theta cycles (Figure 8A; O'Keefe and Recce, 1993; Skaggs et al., 1996; Dragoi and Buzsáki, 2006; Foster and Wilson, 2007). Previous theoretical and experimental work has suggested that during nonspatial memories, the theta phases of spiking activity reflect the animal's behavioral state (Wallenstein and Hasselmo, 1997; Wallenstein et al., 1998; Manns et al., 2007b). In this study, we demonstrate that theta phase information of neuronal spiking also serves as the essential substrate for the representation of the temporal order of discrete events. In our experiments, event neurons discharged with low firing rates on late phases of theta oscillation before event onset (Figure 4; Figure S7). Following onset, we observed transient phase precession followed by sustained phase locking to early theta phases during the remainder of the event period. Moreover, phase precession occurred only for preferred events, while spikes for nonpreferred events were restricted to late theta phases (Figure 4; Figure S7). This transient phase precession and phase locking for preferred events defined a temporal code for discrete event sequences (Figure 8B). Our results indicate that anticipated or nonpreferred information is maintained in late theta phases (ascending phases), while confirmed information is shifted to and sustained in the earlier phases (descending phases) for each event neuron, thus representing temporal order of discrete episodic events within single theta cycles (Figures 6 and 8). Our data support the idea that a common computation framework underlies processing of sequence information for spatial navigation and episodic memory in the hippocampus (O'Keefe and Nadel, 1978; Eichenbaum, 2004; Buzsáki and Moser, 2013).

Sustained Rate Increase and Phase Locking in Discrete Events

The most common pattern of neuronal activity we observed during nonspatial discrete events was sustained rate elevation and phase locking to early theta phases (Figures 2, 3, and 4). As discussed above, we hypothesize that hippocampal neurons represent event components for both spatial and nonspatial episodes (Eichenbaum, 2004). In voluntary behaviors, such as spatial navigation

Figure 6. Theta Sequences of Time and Combination Information

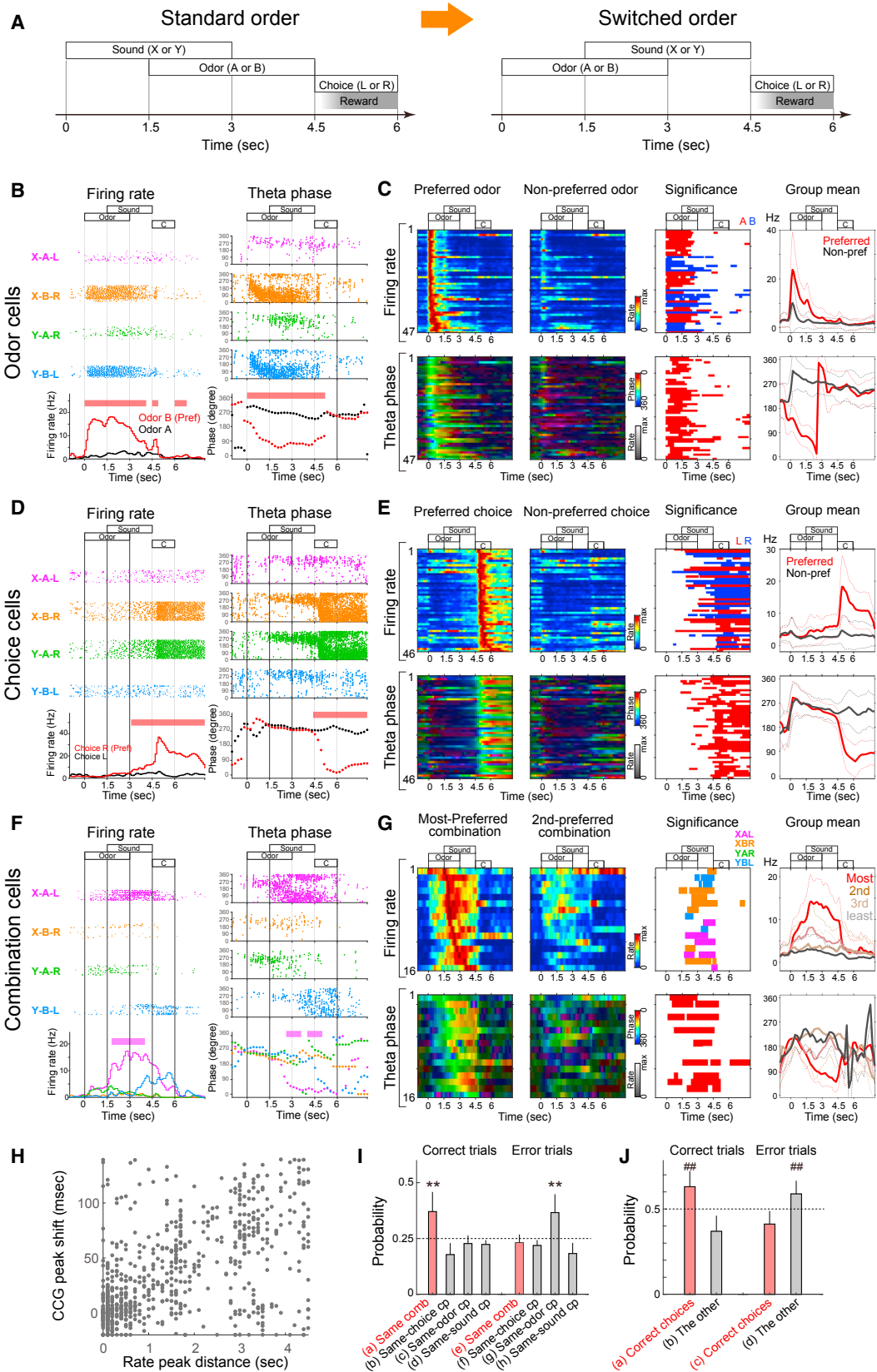
(A) Probability density of time information computed from simultaneously recorded pyramidal cell activities in a single trial (bottom). Bayesian decoding was performed at every 5-ms time step with a 20-ms time window. Top, simultaneously recorded LFP and units from 30 pyramidal neurons ordered by the peak times of their firing rates from bottom to top. See also Figure S10A.

(B) Probability density of time information as a function of theta phase, estimated in the sampling periods 0~1.5 s (sound presentation only), 1.5~3 s (sound and odor presentation), 3~4.5 s (odor presentation only), and 4.5~6 s (choice). This is a representative result from a single session.

(C) Decoded time information (i.e., argument of the maximum of probability densities) as a function of theta phase in single sessions ($n = 24$ sessions; sessions that contained more than 10 pyramidal neurons that displayed phase precession were selected).

(D) Probability densities of the time and combination information as functions of theta phases, estimated from spikes (sampled in time segment 3~4.5 s) in correctly answered (left) and error (right) trials. This is a representative result computed from all trials in a single example session. “Same combinations” means that the sampled spikes and the priors for decoding were from the same type of combination conditions. See also Figure S10B, for other “counterparts.”

(E and F) Decoded probabilities of combination (E) and future choice (F) information in correct and error trials (mean and SD; $n = 17$ sessions; sessions that contained more than 10 pyramidal neurons that displayed phase precession and at least 2 error trials in each combination condition were selected). Probability density functions were computed with spikes in the sampling period 3~4.5 s in single sessions. Decoded probabilities of combination conditions on descending phases (E) and future choices on ascending phases (F) were estimated from ROIs (indicated in insets) taken from the same dataset. ** $p < 0.01$ versus b, c, d, e, f, and h; ### $p < 0.01$ versus b and c; ANOVA and post hoc Tukey-Kramer test.



(legend on next page)

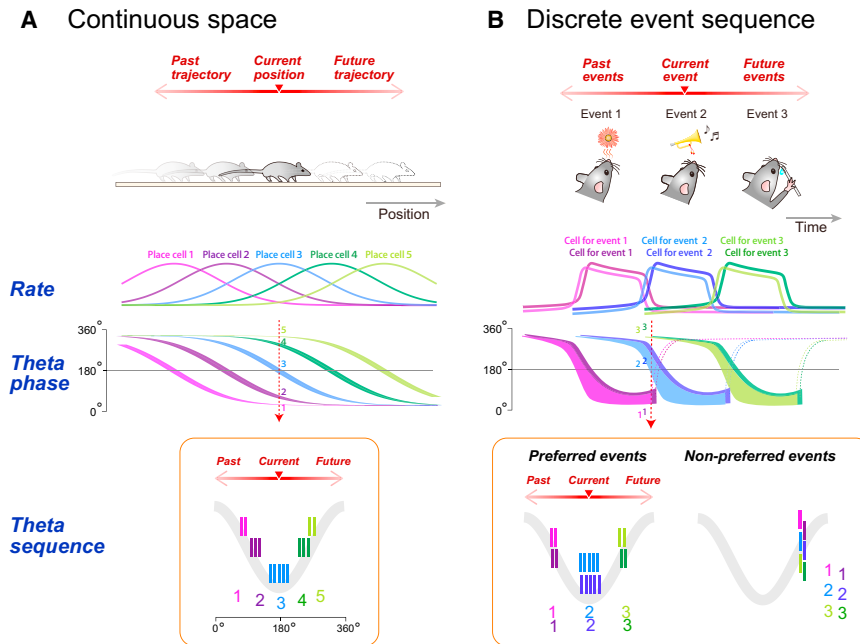


Figure 8. Rate and Temporal Coding for Continuous and Discrete Sequences

(A) For continuous space. Spatial sequences are continuously represented in theta cycles (Dragoi and Buzsáki, 2006).

(B) For discrete events. Event cells show sustained rate increase during preferred events. These neurons displayed transient theta phase precession at the onset of events, followed by phase locking to the early theta phases during the periods of the events. Event sequences of past, current, and future are thus discretely represented in theta cycles.

phase precession, including dual oscillator models (O'Keefe and Burgess, 2005; O'Keefe and Recce, 1993) and soma-dendritic interference models (Kamondi et al., 1998; Magee, 2001). The dual oscillator models hypothesize that two sets of oscillatory inputs with slightly different frequencies interfere to generate beat-like fluctuations, which causes continuous phase shifts of spiking activities on the

theta rhythm. However, this model cannot explain the transient phase precession followed by sustained phase locking observed in our experiments, because the model can only predict continuous phase changes. On the other hand, the soma-dendritic interference model predicts that the interference of tonic somatic theta-rhythm inhibition and ramping up increases of dendritic excitation cause a gradual shift of spiking phases during theta (Harris et al., 2002; Mehta et al., 2002; Harvey et al., 2009; Losonczy et al., 2010). In our experiments with discrete event sequences, we assume that event cells received sustained dendritic inputs during preferred events, since auto-correlations of population vectors showed segmented and sustained network activities during single events (Figure 3C). We hypothesize that the interference of somatic theta-rhythm inhibition and rectangular-type (instead of ramp-up) dendritic excitation would explain the mechanisms of transient phase precession and phase maintenance.

Then, what are the possible physiological mechanisms of the transient phase precession and phase locking? In spatial navigation, several theories have been proposed for continuous

Figure 7. Neuronal Representations When the Order of Cue Presentations Was Switched

(A) Schematic of the new task. The presentation orders of sound and odor cues were switched, without changing the contingencies of combination-choice association (Figure 1B).

(B) Firing rates and theta phases of a representative odor-selective neuron in order-switched trials.

(C) Firing rates and theta phases of all odor-selective neurons in order-switched trials ($n = 47$ units). Top, firing rates of odor-selective neurons during preferred- and nonpreferred-odor trials. Color scale represents firing rate of each neuron. Neurons were ordered by the time of their peak firing rates. Third column shows segments with significantly higher discharge rates in odor-A (red) or odor-B (blue) trials ($p < 0.05$; permutation test). Right column shows mean firing rates (thick line) \pm SD (dotted line). Bottom, theta phases as a function of time during preferred- and nonpreferred-odor trials. Hue represents theta phases (0° – 360°), and brightness represents normalized firing rates in each neuron. Third column shows segments with significantly different phases in different odor trials. ($p < 0.05$ for one side; permutation test). Right column shows mean phases \pm SD.

(D) Firing rates and theta phases of a representative choice-selective neuron in order-switched trials.

(E) Firing rates and theta phases of all choice-selective neurons in order-switched trials ($n = 46$ units).

(F) Firing rates and theta phases of a representative combination-selective neuron in order-switched trials.

(G) Firing rates and theta phases of all combination-selective neurons in order-switched trials ($n = 16$ units).

(H) Pairwise analysis of temporal compression of spike sequence. Each dot represents a single neuronal pair in a single combination. x axis shows peak distances of firing rates and y axis shows peak shifts of CCGs (see Figure 5C). Reference neurons for CCG were the ones whose PSTH peaks were earlier than the others.

(I and J) Decoded probabilities of combination (I) and future choice (J) information in order-switched trials (mean and SD; $n = 6$ sessions). Probability density functions were computed with spikes in the sampling period 3–4.5 s in single sessions. Estimation methods and ROIs for (I) and (J) were same as Figures 6E and 6F, respectively. ** $p < 0.01$ versus b, c, d, e, f, and h; ## $p < 0.01$ versus b and c; ANOVA and post hoc Tukey-Kramer test.

We also observed that fast-spiking neurons showed a transient increase in firing rate at the onset of events with stimulus- and choice-specificity (Figure S3). Since somatostatin and parvalbumin interneurons strongly regulate the firing rates and theta phase timing of pyramidal cells, respectively, in the CA1 (Royer et al., 2012; Amilhon et al., 2015), event-specific firing of fast-spiking neurons could also contribute to phase precession of selected sets of pyramidal neurons (Buzsáki and Chrobak, 1995; Wallenstein and Hasselmo, 1997; Mann and Paulsen, 2007).

In conclusion, the results of this study suggest that a fundamental role of the hippocampus is to order both spatial and nonspatial information across the axes of space and time. Information of events or place is represented by the firing rate of event cells or place cells, while temporal sequence information is carried by the timing of spikes relative to the theta phase (Figure 8). We propose that the theory of rate and temporal coding in the hippocampus (Huxter et al., 2003; Foster and Wilson, 2007; Buzsáki and Moser, 2013) is now a common conceptual framework for both spatial navigation and episodic memory.

STAR★METHODS

Detailed methods are provided in the online version of this paper and include the following:

- KEY RESOURCES TABLE
- CONTACT FOR REAGENT AND RESOURCE SHARING
- EXPERIMENTAL MODEL AND SUBJECT DETAILS
- METHOD DETAILS
 - Behavioral task
 - Surgery and recording
 - Data analysis
- QUANTIFICATION AND STATISTICAL ANALYSIS

SUPPLEMENTAL INFORMATION

Supplemental Information includes one table, eleven figures, and one movie and can be found with this article online at <http://dx.doi.org/10.1016/j.neuron.2017.05.024>.

AUTHOR CONTRIBUTIONS

S.T., Y.S., H.N., and S.F. designed the experiments. H.N., S.T., and S.F. designed the behavioral task. S.T. performed experiments. S.T. and S.F. performed data analysis. S.T. and S.F. wrote the paper.

ACKNOWLEDGMENTS

We thank Asohan Amarasingham for help with data analysis and Thomas McHugh and Charles Yokoyama for comments on the manuscript. We thank Kei Sunouchi and RIKEN Advanced Manufacturing Support Team for supporting fabrication of the custom-made experimental apparatus. This study was supported by the JSPS KAKENHI Grant (26119530, 15H05876, and 16H01519 to S.F.; 16H06570 to H.N.; 14J02824 to S.T.) and the JSPS Research Fellowship for Young Scientists (S.T.).

Received: January 3, 2017

Revised: March 10, 2017

Accepted: May 18, 2017

Published: June 8, 2017

REFERENCES

- Aggleton, J.P., and Brown, M.W. (1999). Episodic memory, amnesia, and the hippocampal-anterior thalamic axis. *Behav. Brain Sci.* 22, 425–444, discussion 444–489.
- Agster, K.L., Fortin, N.J., and Eichenbaum, H. (2002). The hippocampus and disambiguation of overlapping sequences. *J. Neurosci.* 22, 5760–5768.
- Allen, T.A., Salz, D.M., McKenzie, S., and Fortin, N.J. (2016). Nonspatial sequence coding in CA1 neurons. *J. Neurosci.* 36, 1547–1563.
- Amarasingham, A., Harrison, M.T., Hatsopoulos, N.G., and Geman, S. (2012). Conditional modeling and the jitter method of spike resampling. *J. Neurophysiol.* 107, 517–531.
- Amilhon, B., Huh, C.Y., Manseau, F., Ducharme, G., Nichol, H., Adamantidis, A., and Williams, S. (2015). Parvalbumin interneurons of hippocampus tune population activity at theta frequency. *Neuron* 86, 1277–1289.
- Berens, P. (2009). CircStat: a MATLAB toolbox for circular statistics. *J. Stat. Softw.* 31, 1–21.
- Berényi, A., Somogyvári, Z., Nagy, A.J., Roux, L., Long, J.D., Fujisawa, S., Stark, E., Leonardo, A., Harris, T.D., and Buzsáki, G. (2014). Large-scale, high-density (up to 512 channels) recording of local circuits in behaving animals. *J. Neurophysiol.* 111, 1132–1149.
- Brown, E.N., Frank, L.M., Tang, D., Quirk, M.C., and Wilson, M.A. (1998). A statistical paradigm for neural spike train decoding applied to position prediction from ensemble firing patterns of rat hippocampal place cells. *J. Neurosci.* 18, 7411–7425.
- Bunsey, M., and Eichenbaum, H. (1996). Conservation of hippocampal memory function in rats and humans. *Nature* 379, 255–257.
- Burgess, N., Maguire, E.A., and O'Keefe, J. (2002). The human hippocampus and spatial and episodic memory. *Neuron* 35, 625–641.
- Buzsáki, G. (2002). Theta oscillations in the hippocampus. *Neuron* 33, 325–340.
- Buzsáki, G., and Chrobak, J.J. (1995). Temporal structure in spatially organized neuronal ensembles: a role for interneuronal networks. *Curr. Opin. Neurobiol.* 5, 504–510.
- Buzsáki, G., and Moser, E.I. (2013). Memory, navigation and theta rhythm in the hippocampal-entorhinal system. *Nat. Neurosci.* 16, 130–138.
- Cei, A., Girardeau, G., Drieu, C., Kanbi, K.E., and Zugaro, M. (2014). Reversed theta sequences of hippocampal cell assemblies during backward travel. *Nat. Neurosci.* 17, 719–724.
- Csicsvari, J., Hirase, H., Czurko, A., and Buzsáki, G. (1998). Reliability and state dependence of pyramidal cell-interneuron synapses in the hippocampus: an ensemble approach in the behaving rat. *Neuron* 21, 179–189.
- Davidson, T.J., Kloosterman, F., and Wilson, M.A. (2009). Hippocampal replay of extended experience. *Neuron* 63, 497–507.
- Dragoi, G., and Buzsáki, G. (2006). Temporal encoding of place sequences by hippocampal cell assemblies. *Neuron* 50, 145–157.
- Dusek, J.A., and Eichenbaum, H. (1997). The hippocampus and memory for orderly stimulus relations. *Proc. Natl. Acad. Sci. USA* 94, 7109–7114.
- Eichenbaum, H. (2004). Hippocampus: cognitive processes and neural representations that underlie declarative memory. *Neuron* 44, 109–120.
- Eichenbaum, H., and Cohen, N.J. (2014). Can we reconcile the declarative memory and spatial navigation views on hippocampal function? *Neuron* 83, 764–770.
- Eichenbaum, H., Kuperstein, M., Fagan, A., and Nagode, J. (1987). Cue-sampling and goal-approach correlates of hippocampal unit activity in rats performing an odor-discrimination task. *J. Neurosci.* 7, 716–732.
- Feng, T., Silva, D., and Foster, D.J. (2015). Dissociation between the experience-dependent development of hippocampal theta sequences and single-trial phase precession. *J. Neurosci.* 35, 4890–4902.
- Fortin, N.J., Agster, K.L., and Eichenbaum, H.B. (2002). Critical role of the hippocampus in memory for sequences of events. *Nat. Neurosci.* 5, 458–462.

- Foster, D.J., and Wilson, M.A. (2006). Reverse replay of behavioural sequences in hippocampal place cells during the awake state. *Nature* *440*, 680–683.
- Foster, D.J., and Wilson, M.A. (2007). Hippocampal theta sequences. *Hippocampus* *17*, 1093–1099.
- Foster, D.J., and Knierim, J.J. (2012). Sequence learning and the role of the hippocampus in rodent navigation. *Curr. Opin. Neurobiol.* *22*, 294–300.
- Fujisawa, S., Amarasingham, A., Harrison, M.T., and Buzsáki, G. (2008). Behavior-dependent short-term assembly dynamics in the medial prefrontal cortex. *Nat. Neurosci.* *11*, 823–833.
- Geisler, C., Robbe, D., Zugaro, M., Sirota, A., and Buzsáki, G. (2007). Hippocampal place cell assemblies are speed-controlled oscillators. *Proc. Natl. Acad. Sci. USA* *104*, 8149–8154.
- Gothard, K.M., Skaggs, W.E., and McNaughton, B.L. (1996). Dynamics of mismatch correction in the hippocampal ensemble code for space: interaction between path integration and environmental cues. *J. Neurosci.* *16*, 8027–8040.
- Gupta, A.S., van der Meer, M.A., Touretzky, D.S., and Redish, A.D. (2012). Segmentation of spatial experience by hippocampal θ sequences. *Nat. Neurosci.* *15*, 1032–1039.
- Hampson, R.E., Pons, T.P., Stanford, T.R., and Deadwyler, S.A. (2004). Categorization in the monkey hippocampus: a possible mechanism for encoding information into memory. *Proc. Natl. Acad. Sci. USA* *101*, 3184–3189.
- Harris, K.D., Henze, D.A., Hirase, H., Leinekugel, X., Dragoi, G., Czurkó, A., and Buzsáki, G. (2002). Spike train dynamics predicts theta-related phase precession in hippocampal pyramidal cells. *Nature* *417*, 738–741.
- Harvey, C.D., Collman, F., Dombeck, D.A., and Tank, D.W. (2009). Intracellular dynamics of hippocampal place cells during virtual navigation. *Nature* *461*, 941–946.
- Hasselmo, M.E. (2005). What is the function of hippocampal theta rhythm?—linking behavioral data to phasic properties of field potential and unit recording data. *Hippocampus* *15*, 936–949.
- Huxter, J., Burgess, N., and O’Keefe, J. (2003). Independent rate and temporal coding in hippocampal pyramidal cells. *Nature* *425*, 828–832.
- Isomura, Y., Harukuni, R., Takekawa, T., Aizawa, H., and Fukai, T. (2009). Microcircuitry coordination of cortical motor information in self-initiation of voluntary movements. *Nat. Neurosci.* *12*, 1586–1593.
- Kadir, S.N., Goodman, D.F., and Harris, K.D. (2014). High-dimensional cluster analysis with the masked EM algorithm. *Neural Comput.* *26*, 2379–2394.
- Kamondi, A., Acsády, L., Wang, X.J., and Buzsáki, G. (1998). Theta oscillations in somata and dendrites of hippocampal pyramidal cells in vivo: activity-dependent phase-precession of action potentials. *Hippocampus* *8*, 244–261.
- Kimura, R., Saiki, A., Fujiwara-Tsakamoto, Y., Ohkubo, F., Kitamura, K., Matsuzaki, M., Sakai, Y., and Isomura, Y. (2012). Reinforcing operandum: rapid and reliable learning of skilled forelimb movements by head-fixed rodents. *J. Neurophysiol.* *108*, 1781–1792.
- Komorowski, R.W., Manns, J.R., and Eichenbaum, H. (2009). Robust conjunctive item-place coding by hippocampal neurons parallels learning what happens where. *J. Neurosci.* *29*, 9918–9929.
- Kraus, B.J., Robinson, R.J., 2nd, White, J.A., Eichenbaum, H., and Hasselmo, M.E. (2013). Hippocampal “time cells”: time versus path integration. *Neuron* *78*, 1090–1101.
- Lenck-Santini, P.P., Fenton, A.A., and Muller, R.U. (2008). Discharge properties of hippocampal neurons during performance of a jump avoidance task. *J. Neurosci.* *28*, 6773–6786.
- Leutgeb, S., Leutgeb, J.K., Barnes, C.A., Moser, E.I., McNaughton, B.L., and Moser, M.B. (2005). Independent codes for spatial and episodic memory in hippocampal neuronal ensembles. *Science* *309*, 619–623.
- Lisman, J. (2005). The theta/gamma discrete phase code occurring during the hippocampal phase precession may be a more general brain coding scheme. *Hippocampus* *15*, 913–922.
- Losonczy, A., Zemelman, B.V., Vaziri, A., and Magee, J.C. (2010). Network mechanisms of theta related neuronal activity in hippocampal CA1 pyramidal neurons. *Nat. Neurosci.* *13*, 967–972.
- MacDonald, C.J., Lepage, K.Q., Eden, U.T., and Eichenbaum, H. (2011). Hippocampal “time cells” bridge the gap in memory for discontinuous events. *Neuron* *71*, 737–749.
- Magee, J.C. (2001). Dendritic mechanisms of phase precession in hippocampal CA1 pyramidal neurons. *J. Neurophysiol.* *86*, 528–532.
- Mann, E.O., and Paulsen, O. (2007). Role of GABAergic inhibition in hippocampal network oscillations. *Trends Neurosci.* *30*, 343–349.
- Manns, J.R., Howard, M.W., and Eichenbaum, H. (2007a). Gradual changes in hippocampal activity support remembering the order of events. *Neuron* *56*, 530–540.
- Manns, J.R., Zilli, E.A., Ong, K.C., Hasselmo, M.E., and Eichenbaum, H. (2007b). Hippocampal CA1 spiking during encoding and retrieval: relation to theta phase. *Neurobiol. Learn. Mem.* *87*, 9–20.
- McKenzie, S., Frank, A.J., Kinsky, N.R., Porter, B., Rivière, P.D., and Eichenbaum, H. (2014). Hippocampal representation of related and opposing memories develop within distinct, hierarchically organized neural schemas. *Neuron* *83*, 202–215.
- McNaughton, B.L., Battaglia, F.P., Jensen, O., Moser, E.I., and Moser, M.B. (2006). Path integration and the neural basis of the ‘cognitive map’. *Nat. Rev. Neurosci.* *7*, 663–678.
- Mehta, M.R., Lee, A.K., and Wilson, M.A. (2002). Role of experience and oscillations in transforming a rate code into a temporal code. *Nature* *417*, 741–746.
- Middleton, S.J., and McHugh, T.J. (2016). Silencing CA3 disrupts temporal coding in the CA1 ensemble. *Nat. Neurosci.* *19*, 945–951.
- Mizuseki, K., Sirota, A., Pastalkova, E., and Buzsáki, G. (2009). Theta oscillations provide temporal windows for local circuit computation in the entorhinal-hippocampal loop. *Neuron* *64*, 267–280.
- Mizuseki, K., Diba, K., Pastalkova, E., and Buzsáki, G. (2011). Hippocampal CA1 pyramidal cells form functionally distinct sublayers. *Nat. Neurosci.* *14*, 1174–1181.
- Naya, Y., and Suzuki, W.A. (2011). Integrating what and when across the primate medial temporal lobe. *Science* *333*, 773–776.
- O’Keefe, J., and Dostrovsky, J. (1971). The hippocampus as a spatial map. Preliminary evidence from unit activity in the freely-moving rat. *Brain Res.* *34*, 171–175.
- O’Keefe, J., and Nadel, L. (1978). *The Hippocampus as a Cognitive Map* (Oxford University Press).
- O’Keefe, J., and Recce, M.L. (1993). Phase relationship between hippocampal place units and the EEG theta rhythm. *Hippocampus* *3*, 317–330.
- O’Keefe, J., and Burgess, N. (2005). Dual phase and rate coding in hippocampal place cells: theoretical significance and relationship to entorhinal grid cells. *Hippocampus* *15*, 853–866.
- O’Reilly, R.C., and Rudy, J.W. (2001). Conjunctive representations in learning and memory: principles of cortical and hippocampal function. *Psychol. Rev.* *108*, 311–345.
- Pastalkova, E., Itskov, V., Amarasingham, A., and Buzsáki, G. (2008). Internally generated cell assembly sequences in the rat hippocampus. *Science* *321*, 1322–1327.
- Paz, R., Gelbard-Sagiv, H., Mukamel, R., Harel, M., Malach, R., and Fried, I. (2010). A neural substrate in the human hippocampus for linking successive events. *Proc. Natl. Acad. Sci. USA* *107*, 6046–6051.
- Pfeiffer, B.E., and Foster, D.J. (2013). Hippocampal place-cell sequences depict future paths to remembered goals. *Nature* *497*, 74–79.
- Quiroga, R.Q., Reddy, L., Kreiman, G., Koch, C., and Fried, I. (2005). Invariant visual representation by single neurons in the human brain. *Nature* *435*, 1102–1107.
- Royer, S., Zemelman, B.V., Losonczy, A., Kim, J., Chance, F., Magee, J.C., and Buzsáki, G. (2012). Control of timing, rate and bursts of hippocampal place cells by dendritic and somatic inhibition. *Nat. Neurosci.* *15*, 769–775.

- Sakurai, Y. (1990). Hippocampal cells have behavioral correlates during the performance of an auditory working memory task in the rat. *Behav. Neurosci.* *104*, 253–263.
- Sakurai, Y. (1996). Hippocampal and neocortical cell assemblies encode memory processes for different types of stimuli in the rat. *J. Neurosci.* *16*, 2809–2819.
- Skaggs, W.E., McNaughton, B.L., Wilson, M.A., and Barnes, C.A. (1996). Theta phase precession in hippocampal neuronal populations and the compression of temporal sequences. *Hippocampus* *6*, 149–172.
- Squire, L.R., and Zola-Morgan, S. (1991). The medial temporal lobe memory system. *Science* *253*, 1380–1386.
- Sutherland, R.J., and Rudy, J.W. (1989). Configural association theory: the role of the hippocampal-formation in learning, memory, and amnesia. *Psychobiology* *17*, 129–144.
- Takahashi, M., Nishida, H., Redish, A.D., and Lauwereyns, J. (2014). Theta phase shift in spike timing and modulation of gamma oscillation: a dynamic code for spatial alternation during fixation in rat hippocampal area CA1. *J. Neurophysiol.* *111*, 1601–1614.
- Terrazas, A., Krause, M., Lipa, P., Gothard, K.M., Barnes, C.A., and McNaughton, B.L. (2005). Self-motion and the hippocampal spatial metric. *J. Neurosci.* *25*, 8085–8096.
- Tolman, E.C. (1948). Cognitive maps in rats and men. *Psychol. Rev.* *55*, 189–208.
- Tsodyks, M.V., Skaggs, W.E., Sejnowski, T.J., and McNaughton, B.L. (1996). Population dynamics and theta rhythm phase precession of hippocampal place cell firing: a spiking neuron model. *Hippocampus* *6*, 271–280.
- Tulving, E., and Markowitsch, H.J. (1998). Episodic and declarative memory: role of the hippocampus. *Hippocampus* *8*, 198–204.
- Wallenstein, G.V., and Hasselmo, M.E. (1997). GABAergic modulation of hippocampal population activity: sequence learning, place field development, and the phase precession effect. *J. Neurophysiol.* *78*, 393–408.
- Wallenstein, G.V., Eichenbaum, H., and Hasselmo, M.E. (1998). The hippocampus as an associator of discontiguous events. *Trends Neurosci.* *21*, 317–323.
- Wang, Y., Romani, S., Lustig, B., Leonardo, A., and Pastalkova, E. (2015). Theta sequences are essential for internally generated hippocampal firing fields. *Nat. Neurosci.* *18*, 282–288.
- Watanabe, M. (1986a). Prefrontal unit activity during delayed conditional Go/No-Go discrimination in the monkey. I. Relation to the stimulus. *Brain Res.* *382*, 1–14.
- Watanabe, M. (1986b). Prefrontal unit activity during delayed conditional Go/No-Go discrimination in the monkey. II. Relation to Go and No-Go responses. *Brain Res.* *382*, 15–27.
- Wiener, S.I., Paul, C.A., and Eichenbaum, H. (1989). Spatial and behavioral correlates of hippocampal neuronal activity. *J. Neurosci.* *9*, 2737–2763.
- Wikenheiser, A.M., and Redish, A.D. (2015). Hippocampal theta sequences reflect current goals. *Nat. Neurosci.* *18*, 289–294.
- Wills, T.J., Lever, C., Cacucci, F., Burgess, N., and O'Keefe, J. (2005). Attractor dynamics in the hippocampal representation of the local environment. *Science* *308*, 873–876.
- Wirth, S., Yanike, M., Frank, L.M., Smith, A.C., Brown, E.N., and Suzuki, W.A. (2003). Single neurons in the monkey hippocampus and learning of new associations. *Science* *300*, 1578–1581.
- Wood, E.R., Dudchenko, P.A., and Eichenbaum, H. (1999). The global record of memory in hippocampal neuronal activity. *Nature* *397*, 613–616.
- Zhang, K., Ginzburg, I., McNaughton, B.L., and Sejnowski, T.J. (1998). Interpreting neuronal population activity by reconstruction: unified framework with application to hippocampal place cells. *J. Neurophysiol.* *79*, 1017–1044.

STAR★METHODS

KEY RESOURCES TABLE

| REAGENT or RESOURCE | SOURCE | IDENTIFIER |
|---|-------------------------|---|
| Chemicals, Peptides, and Recombinant Proteins | | |
| Hexyl acetate | Tokyo Chemical Industry | Cat# A0032 |
| (-)-menthone | Tokyo Chemical Industry | Cat# M0513 |
| Cuminaldehyde | Tokyo Chemical Industry | Cat# I0168 |
| Experimental Models: Organisms/Strains | | |
| Rat (Long-Evans) | Japan SLC | Cat# Iar:Long-Evans |
| Software and Algorithms | | |
| MATLAB | Mathworks | https://www.mathworks.com/ |
| Circular Statistics Toolbox | Berens, 2009 | https://jp.mathworks.com/matlabcentral/fileexchange/10676-circular-statistics-toolbox-directional-statistics- |
| KlustaKwik2 | Kadir et al., 2014 | https://github.com/kwikteam/klustakwik2 |
| LabVIEW | National Instruments | http://www.ni.com/en-us.html |
| Other | | |
| Silicon probe: 64-sites: 8-shank probe | NeuroNexus | Buzsaki64 |
| Silicon probe: 64-sites: 6-shank probe | NeuroNexus | Buzsaki64sp |
| 256 channel Multiplexed Biosignal Amplifier | Amplipex | KJE-1001 |
| Head-restrained operant apparatus | O'hara | http://ohara-time.co.jp/tag/taskforcer/ |

CONTACT FOR REAGENT AND RESOURCE SHARING

Further information and requests for resources and reagents should be directed to and will be fulfilled by the Lead Contact, Dr. Shigeyoshi Fujisawa (fujisawa@brain.riken.jp).

EXPERIMENTAL MODEL AND SUBJECT DETAILS

Four male Long-Evans rats (Long-Evans, 10~12 months old) were used in this study. All experimental protocols were approved by the RIKEN Institutional Animal Care and Use Committee.

METHOD DETAILS

Behavioral task

Adult male rats were trained in the cue-combination task prior to surgery. It is a decision making task involving integrations of sound and odor cues which are associated with the left or right spout levers under head-restrained condition (Figure 1; Figure S1; Movie S1).

The task training was performed with the computer-controlled operant apparatus (Figure S1) which was modified from TaskForcer (O'hara, Tokyo, Japan; Isomura et al., 2009; Kimura et al., 2012). The left and right spout levers were mounted on the liner-actuators with stepper motors, so that the positions of the levers can be quickly and precisely controlled with pulse signals. Sound stimuli were provided by the speaker placed in front of the rat. Odor stimuli was provided from the custom-made nose cover on air flow (~0.5 l/min), which onset and offset were controlled by solenoid valves. The system was automatically controlled by the custom-written LabVIEW (National Instruments, Austin, TX) programs during the trials. For each rat, same sets of sound cues (two were selected from 4 kHz sine wave, 11 kHz sine wave, mixture of 11 kHz sine wave & 11.5 kHz rectangular waves, or white noise) and odor cues (two were selected from hexyl acetate, (-)-menthone, or cuminaldehyde) were used for all sessions. Prior to starting training of the task, a sliding head attachment was surgically attached to the skull (Isomura et al., 2009; Kimura et al., 2012) and ground and reference screws for electrophysiology were implanted above the cerebellum.

A task trial was initiated from a sound cue, which was presented during the period 0–3.0 s from a trial onset, and then an odor cue was presented during the period 1.5–4.5 s (Figure 1). After the offset of the odor presentation, the left and right spout levers moved to accessible position to the rats so that they can make a choice action, that is, pulling left or right lever. If the choice was correct, water

drops (25 μ l) were delivered from the tip of the lever (Kimura et al., 2012). Inter-trial intervals were \sim 15 s after correctly answered trials and 40–60 s after error trials. The rats performed 100–200 trials in a single session in a day. The rats were deprived of drinking water in their home cages, though access to food was not restricted. Sufficient water was provided in the task as a reward and also one hour after the task.

Training periods of rats for this task were 7–9 weeks. In the first stages of leaning, the odor cues were randomly presented in each trial whereas the auditory cue was fixed one type of sound (i.e., odor-discrimination task in one sound context; \sim 1 week). In the second stage, the auditory cue was now fixed to the other type of sound (i.e., reverse leaning of odor-discrimination task in the other sound context; \sim 1 week). In the third stage, we repeat this process but gradually decrease the numbers of sessions between reversals of sound cues (\sim 2 weeks). In the fourth stage, we introduced sound reversal within a single session. We gradually increase the frequency of sound reversals in a session (\sim 2 weeks). In the last stage, presentations of sound and odor cues were totally randomized (\sim 2 weeks). Rats with performances better than 80% correct choices for each combination condition in a single session were chosen for surgery for chronic recording.

Surgery and recording

Four rats (rat-id: t14, t24, t27, and t29) were implanted with silicon probes for chronic recording of neuronal activities during the task behavior. General surgical procedures for chronic recordings have been described in the previous paper (Fujisawa et al., 2008). In this study, Buzsaki64 or Buzsaki64sp types of silicon probes (NeuroNexus, Ann Arbor, MI) were used, which consisted of 8 or 6 shanks (200- μ m shank separation) and each shank had 8 or 10 recording sites (160 μ m² each site; \sim 1 M Ω impedance), respectively, staggered to provide a two-dimensional arrangement (20 μ m vertical separation; see, Figure S1D inset). The rats were implanted with 1–4 silicon probes in the CA1 (rat-t14 with 1 probe at AP = -3.7 mm, ML = 2.7 mm; rat-t24 and t27 with 2 probes at AP = -3.7 mm, ML = \pm 2.7 mm; rat-t29 with 4 probes at AP = -3.0 mm, ML = \pm 2.0 mm & AP = -4.2 mm, ML = \pm 3.4 mm; The shanks were aligned parallel to the septotemporal axis of the hippocampus, i.e., 45 degrees parasagittal). The silicon probe was attached to a micromanipulator and moved gradually to its desired depth position. During the recording sessions, the wide-band neurophysiological signals were acquired continuously at 20 kHz on a 256-channel Ampliplex systems (KJE-1001, Ampliplex Ltd, Hungary; Berényi et al., 2014). The wide-band signal was downsampled to 1.25 kHz and used as the local field potential (LFP) signal. Spike sorting was performed semi-automatically, using KlustaKwik2 (Kadir et al., 2014), followed by manual adjustment of the clusters. The probes were moved by experimenter with 30–60 μ m until it reached the pyramidal cell layer. After it reached the layer, the probe was stopped or moved with less than 15 μ m for maximizing the numbers of recording units. Even when the experimenter did not move the probe, the tips of the probes spontaneously moved slightly between sessions, which was inferred from the small differences of the waveforms of units across different sessions. We cannot exclude the possibility that some neurons recorded in different sessions were identical because spikes from sessions recorded on different days were clustered separately. Thus, the total number of independent neurons could be overestimated (Mizuseki et al., 2009).

Data analysis

All analyses after spike sorting were performed using custom-written tools in MATLAB with Signal-processing and Statistic toolboxes (Mathworks, Natick, MA). The Circular Statistics Toolbox (Berens, 2009) was used for circular analyses.

Permutation tests (two conditions)

Permutation tests were used to identify conditional differences in firing rates or firing phases in the trial periods (Figures 2, 3, 4, and 7; Figures S3, S6, S9, and S11). Detailed information of this method is described in Figure S2 and the previous papers (Fujisawa et al., 2008; Amarasingham et al., 2012).

The PSTH was estimated from the onset of sound stimulus in each condition, (for example, Odor A and B conditions; $\lambda_A(t)$ and $\lambda_B(t)$), with smoothing using Gaussian kernel function of bandwidth $\sigma = 150$ ms. Then, the difference of PSTHs, $D_0(t) = \lambda_A(t) - \lambda_B(t)$ were computed. The Odor A/B assignments to the labels of sessions were randomly permuted, and the PSTHs and the statistic $D_1(t)$ under the permuted labels were re-estimated. This process was repeated R times to obtain the statistic from the original data, $D_0(x)$, along with the statistic from resample data, $D_1(t), \dots, D_R(t)$. Using this resampled (shuffled) dataset, pointwise p value (5% for both side, i.e., 2.5% for upper and lower) at each point was computed. To avoid multiple comparison issues, we also computed the global 5% bands (Figure S2; Fujisawa et al., 2008).

To assess conditional differences of spiking phases as a function of time in each unit, the difference of mean spiking phases in each time bin was computed as the same way ($p < 0.05$ for one side, since there is no directionality for phase difference).

Permutation tests (four conditions)

When we assessed the differences of the firing rates among four combination conditions, the preferences of combinations for each cells were ordered based on their peak firing rates in each combination condition, that is, most-, 2nd-most-, 3rd-most-, and least-preferred combination conditions. Then, permutation tests described above were applied to compare most- versus 2nd-most-, most- versus 3rd-most-, and most- versus least-preferred combination trials. We determined that the firing rates in most-preferred

was significantly highest if all of the three comparisons had significant differences. Bonferroni correction was applied for each comparison, i.e., $p < 0.05/3 = 0.0167$ for each permutation test.

Assessment of differences of spiking phases as a function of time in four combination conditions for each unit was performed as the same way.

Population vector analysis

First, the normalized PSTH for each neuron was computed in each combination condition. Then, the population vector matrix of all pyramidal neurons (i.e., a single row vector represents a normalized PSTH in a single neuron, and a column vector represents a population vector of all neurons at a single time bin) was constructed in each combination condition. Finally, the autocorrelation of the population vector matrix in each combination condition was computed (Figure 3C). Here, the element at point (i, j) represents the Pearson's correlation coefficient between the population vectors computed at i-th and j-th time bin in the trials (Gothard et al., 1996). Cross-correlations of the population vectors were also computed in the same way. The detailed procedures of computation is also explained in Figure S5C.

Analysis of LFP

For the theta phase extraction, LFPs in the CA1 pyramidal cell layers (which were determined by the amplitudes of ripples and the polarities of sharp-waves; Mizuseki et al., 2011) were filtered with a Butterworth filter with pass-band range 4-10 Hz. Instantaneous theta phases were estimated by Hilbert transformation of the filtered signals.

The presence of theta phase precession was assessed in each neuron in each combination condition, with using following three criteria (Figure S6C); (i) there was a significant liner-circular correlation ($p < 0.01$) between time and theta phases, in the period between -1.5 s to 1.5 s of the time of the peak firing rate, (ii) the phases crossed 180° (troughs of theta) in the period between -1.5 s to 1.5 s of peak time, and (iii) the phase shift was more than 120° .

Pairwise analysis of theta sequences

Pairwise analysis of theta sequences was applied to the cell pairs in single conditions (Figure 5C). The cell pairs and conditions were selected with following criteria; (i) both neurons had phase precessions in the combination condition, and (ii) the cross-correlogram (CCG) of the cell pair in the combination condition had significant theta modulation. Significance of theta modulation of CCG was assessed as follows. First, we computed the Fourier power of CCG of a cell pair. Second, the trial labels of the raster plot of each cell were shuffled (i.e., shift predictor), in order to break precise temporal relationships of spikes of cell pairs with preserving their PSTHs. Then we computed Fourier power of CCG with using the surrogate spike trains. We repeated to make surrogate CCGs for 200 times. If the theta-band power of original CCG was higher than 5% top of those of surrogate CCGs, we considered that theta modulation is significant ($p < 0.05$).

Reconstruction of time and combination from neuronal activities

A memoryless Bayesian decoding algorithm was used to estimate the information of time and combination of a task trial which the animal was engaged in, based on the combination-specific PSTHs and the spike trains (Figure 6; Figure S10; Davidson et al., 2009; Feng et al., 2015; Zhang et al., 1998; Brown et al., 1998). Based on the Bayes' theory, the posterior probability of time from a trial onset (*time*) and combination conditions (*comb*) given spike trains from single neurons (*spikes*) was estimated as:

$$P(\text{time, comb} | \text{spikes}) = \frac{P(\text{spikes} | \text{time, comb}) \cdot P(\text{time, comb})}{P(\text{spikes})}$$

The prior probability was estimated under the assumption of Poisson firing statistics and independent rates, as:

$$P(\text{spikes} | \text{time, comb}) = \prod_{i=1}^N P(n_i | \text{time, comb}) = \prod_{i=1}^N \frac{(\tau f_i(\text{time, comb}))^{n_i}}{n_i!} \exp(-\tau f_i(\text{time, comb}))$$

where τ is the time window of sampling spike trains (20ms, moving with 5ms step, was used in this study), $f_i(\text{time, comb})$ is the PSTH of *i*-th unit in each combination condition (e.g., Figure S10A), n_i is the number of spikes of *i*-th unit in the time window, and N is the total number of units. Combining these equations, the posterior probability of the time and combination was computed as:

$$P(\text{time, comb} | \text{spikes}) = C \cdot P(\text{time, comb}) \left(\prod_{i=1}^N \frac{(\tau f_i(\text{time, comb}))^{n_i}}{n_i!} \right) \exp\left(-\tau \sum_{i=1}^N f_i(\text{time, comb})\right)$$

where C is a normalization factor which depends on τ and the numbers of spikes of each neuron (Zhang et al., 1998). To construct theta sequences, decoded probabilities over trials were aligned to the theta phases calculated from concurrently recorded LFP and were averaged (Davidson et al., 2009; Feng et al., 2015).

When only the information of *time* was reconstructed (Figures 6A–6C), the posterior probability of time in which the combination parameters were conditioned, i.e., (*time* | *spikes*, *comb*), was estimated. In Figure 6C, the most probable time was taken as the reconstructed time, i.e., $\hat{t} = \underset{\text{time}}{\operatorname{argmax}} P(\text{time} | \text{spikes}, \text{comb})$, in order to show session-to-session variability.

For these analyses, we selected the sessions in which more than 10 simultaneously-recorded pyramidal neurons which had phase precession in at least one single combination condition ($n = 24$ sessions). For comparison correct and error trials (Figures 7E and 7F), we selected the sessions had more than 10 pyramidal neurons with phase precession and at least 2 error trials in each combination condition ($n = 17$ sessions).

QUANTIFICATION AND STATISTICAL ANALYSIS

All statistical analyses were performed in MATLAB. Details of statistical analyses were described in METHOD DETAILS section.

Neuron, Volume 94

Supplemental Information

**Temporal and Rate Coding for Discrete
Event Sequences in the Hippocampus**

Satoshi Terada, Yoshio Sakurai, Hiroyuki Nakahara, and Shigeyoshi Fujisawa

SUPPLEMENTARY TABLE

Table S1. Basic physiology statistics, related to Figures 2~7.

| | Standard task (Figures 2~6) | Order-switched ⁶⁾ (Figure 7) | 1st-day of switch (Figure S11) |
|---|--------------------------------|--|-----------------------------------|
| Rats | t14, t24, t27, t29 | t27, t29 | t27, t29 |
| Total sessions | 34 | 6 | 2 |
| Total pyramidal cells ¹⁾ | 754 | 190 | 66 |
| Peak firing rate of pyr cells (Hz) | 16.3±7.0 | 18.2±5.7 | 16.8±7.6 |
| Total pyr cells with TPP ²⁾ | 472 | 109 | 34 |
| Total odor-selective pyr cells ³⁾ | 152 | 47 | 16 |
| Total choice-selective pyr cells ⁴⁾ | 222 | 46 | 11 |
| Total combination-selective pyr cells ⁵⁾ | 72 | 16 | - |
| Number of pyr cells per session | 22.2±13.1 | 31.7±3.6 | 33.0±7.1 |
| Number of TPP pyr cells per session | 13.9±8.0 | 17.7±8.9 | 17.0±12.7 |

1) Pyramidal cells which peak firing rates were more than 8 Hz were selected. See also, Figure S1C.

2) Criteria of theta phase precession (TPP) are described in Figure S6C.

3) Odor-selective neurons were defined as neurons which had significant rate differences between Odor-A and B trials in odor-representing periods. See, Figure 4A, B.

4) Choice-selective neurons were defined as neurons which had significant rate differences between Choice-L and R trials in choice periods. See, Figure 4C, D.

5) Combination-selective neurons were defined as neurons which had significant higher rates in specific combinations in sound-and-odor presentation periods. See, Figure 4E, F.

6) Order-switched sessions include ones with more than 75% performance. See, Figure S11A.

SUPPLEMENTARY FIGURES

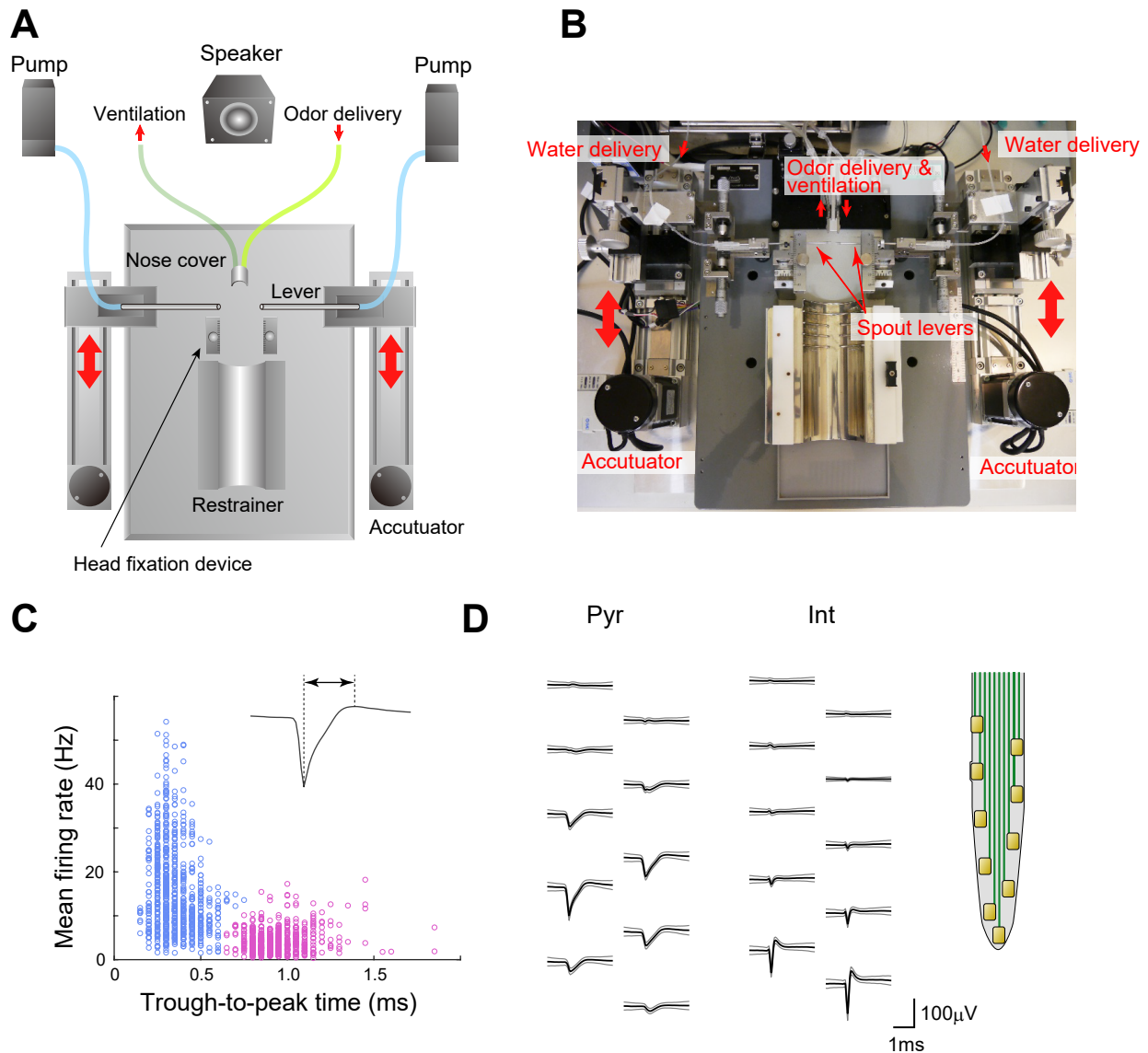


Figure S1. Experimental apparatus and unit classification methods, related to Figure 1.

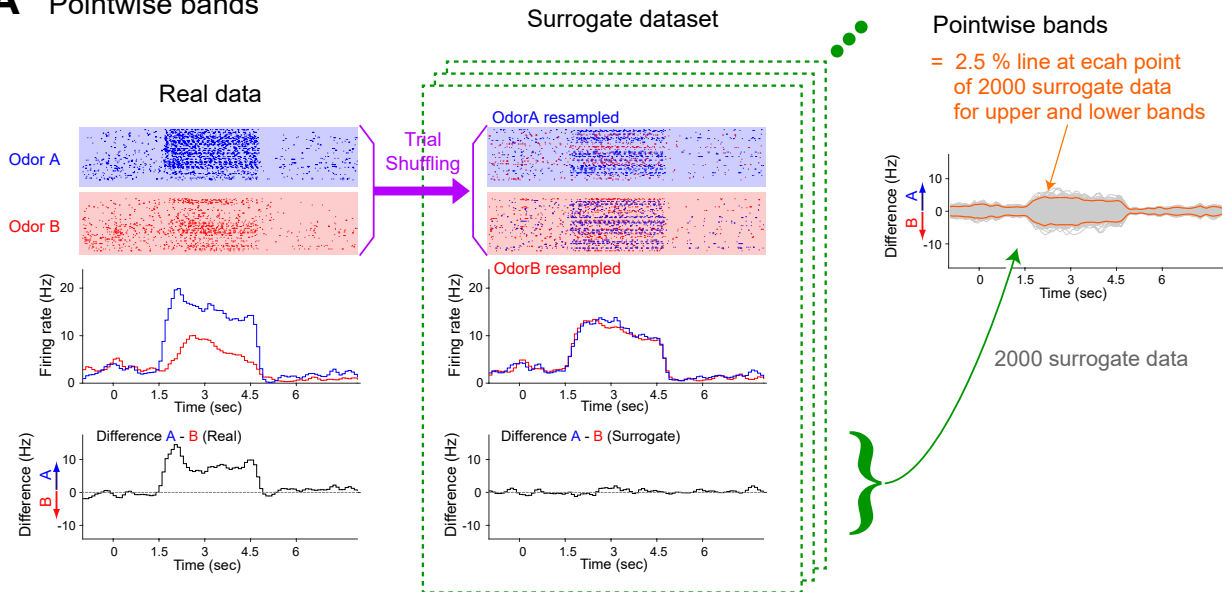
(A) Schematics of behavioral experimental apparatus for the cue-combination task.

(B) Photograph of the experimental apparatus. See also Movie S1.

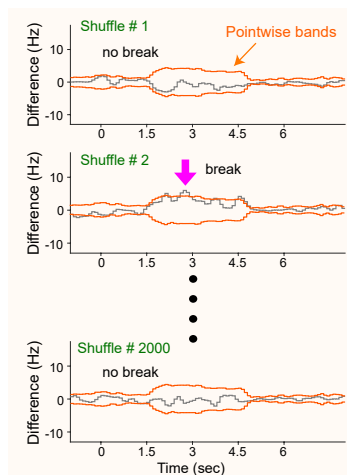
(C) Classification of units into putative pyramidal neurons and interneurons, with using the mean firing rates and shapes of the waveforms. Red and blue dots indicate the units classified into putative pyramidal neurons and interneurons, respectively.

(D) Representative waveforms of a putative pyramidal neuron and interneuron. Inset indicates channel alignment of one shank (10 channels) of a silicon probe. Thick lines indicate mean traces and thin lines indicate SD.

A Pointwise bands



B Global bands



How many data break 2.5% pointwise bands at ANY point ?

If 18.8 % of them break the 2.5%-line, then Pointwise 2.5% bands = Global 18.8 % bands

| Pointwise bands | Global bands |
|-----------------|--------------|
| 2.5 % | 18.8 % |
| 2 % | 14.5 % |
| 1 % | 7.1 % |
| 0.7 % | 4.9 % |
| 0.5 % | 2.9 % |
| 0.4 % | 2.5 % |

Pointwise 0.4% bands = Global 2.5 % bands

Real data vs statistical bands

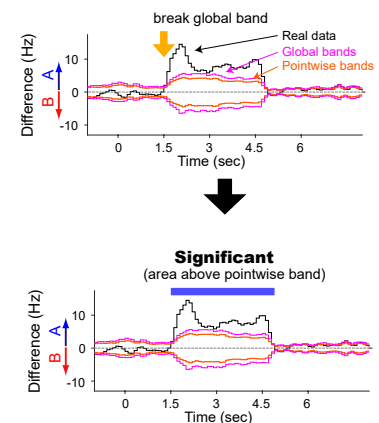


Figure S2. Procedures of a permutation test, related to STAR Methods 'Permutation tests'

(see also, Fujisawa et al., 2008)

(A) PSTH in each condition (i.e. Odor-A and B trials, $\lambda_A(t)$, $\lambda_B(t)$) is computed as a function of time from trial onset. Then we compute the difference of the PSTHs, $D_0(t) = \lambda_A(t) - \lambda_B(t)$. We then randomly permute the Odor-A/B assignments, and re-estimate the PSTHs and compute the statistic $D_1(x)$ under the permuted labels. Repeat this process R times to obtain the statistic from the original data, $D_0(x)$, along with the statistic from resample data, $D_1(x)$, ..., $D_R(x)$. Using resampled (shuffled) data set, we compute pointwise bands. At each time point, we rank surrogate dataset and took 2.5% points from the top and bottom. This is considered as 5% pointwise bands for both sides.

(B) How to compute global bands. Here the adjusted p-values are computed as following. First, create a family of pointwise acceptance band, one for each possible level of significance. Then, for each pointwise acceptance band see what fraction of the samples lie completely within the band. This fraction is that band's simultaneous acceptance level. The adjusted p-value at an index x can be inferred from the smallest level simultaneous acceptance band that does not contain the original measurement at index x . In the example of this figure, the global 2.5% bands correspond to pointwise 0.4% bands. Using the global assessment method, we can establish the lengths of maze segments in our experiments, where spike trains during right and left turns differed significantly. For all neurons, we calculate the shuffled mean, pointwise and global statistics. We determine a segment as significant if it satisfied the global criteria of significance but, once established as significant, pointwise criteria are used to determine the segment's (time) extent.

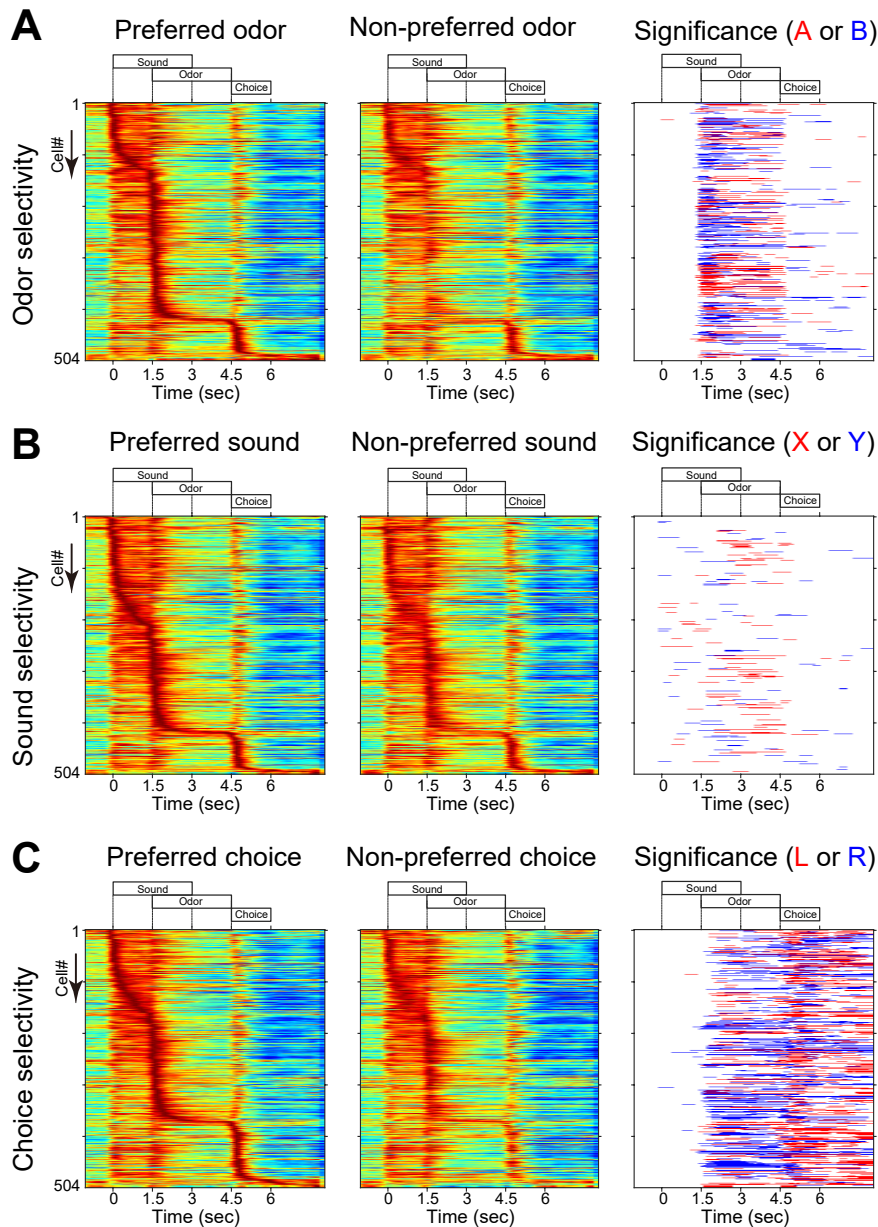


Figure S3. Odor-, sound-, or choice-selective firing activity of CA1 interneurons, related to Figure 2.

(A) Firing patterns of CA1 interneurons during preferred (first column) and non-preferred odor (second column) trials (n=504 units). Each row represents the PSTH of a single neuron (normalized relative to its peak firing rate). Neurons were ordered by the time of their peaks of firing rates. Third column shows segments with significantly higher discharge rates during Odor-A (blue) or Odor-B (red) trials. 70.4 % of interneurons had significantly different discharge rates in odor presenting periods (1.5~4.5 sec) ($P < 0.05$; permutation test).

(B) Firing patterns of CA1 interneurons during preferred (first column) and non-preferred sound (second column) trials (same neuronal sets as A). 19.3% for period 0~3sec; pyramidal 4.5% and interneuron 5.8% for period 0~1.5sec.

(C) Firing patterns of CA1 interneurons during preferred (first column) and non-preferred (second column) choice trials (same neuronal sets as A). 80.6 % of interneurons had significantly different discharge rates ($P < 0.05$).

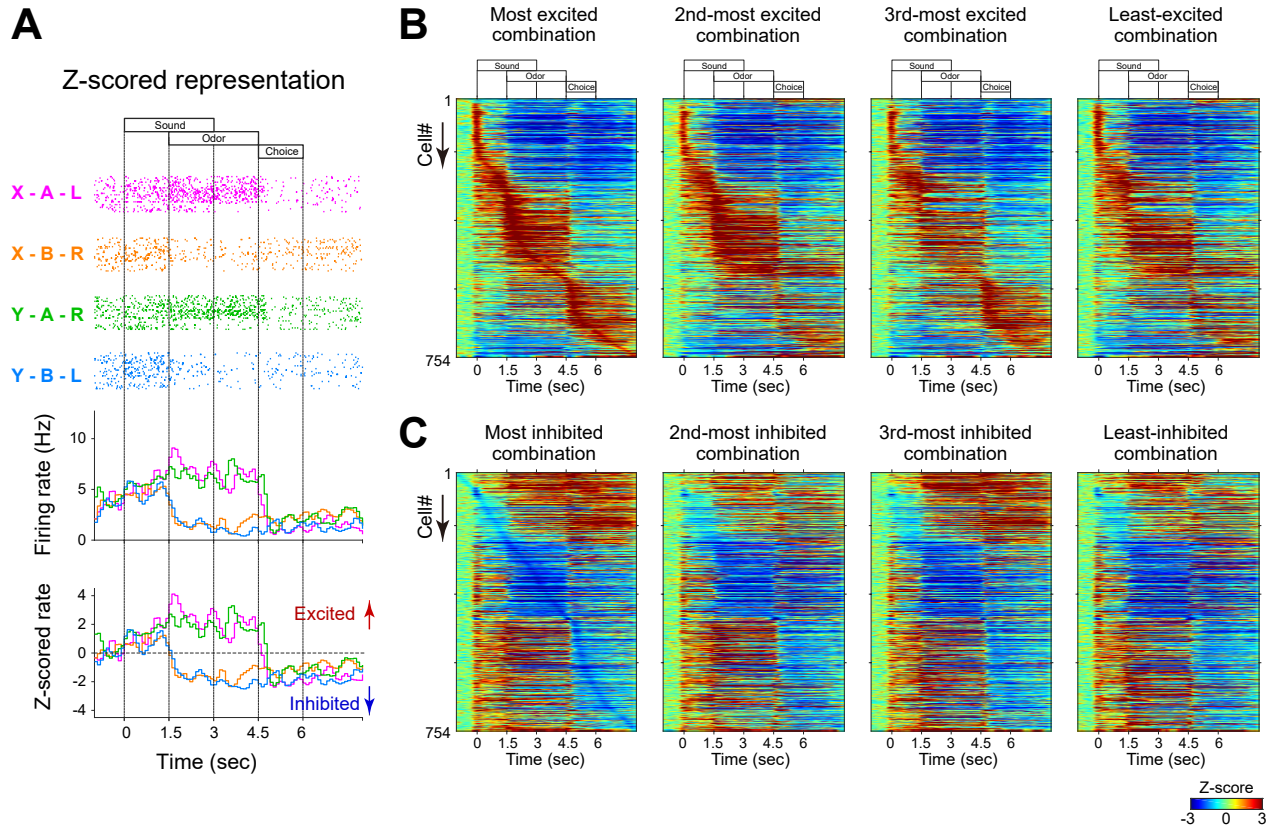


Figure S4. Z-scored firing rates of pyramidal neurons in each combination condition, related to Figure 3.

(A) Firing patterns of CA1 pyramidal neurons were z-scored based on their baseline activity (period -1~0 sec). Z-scored representations of firing rates revealed that CA1 neurons showed either/both stimulus-induced excitation or/and inhibition depending on combination conditions.

(B) Z-scored firing rate plots of all pyramidal neurons ($n=754$ units) in each combination condition. The neurons were sorted based on the times of their peak firing rates.

(C) Same data of (B), but the neurons were sorted based on the times of their minimum firing rates.

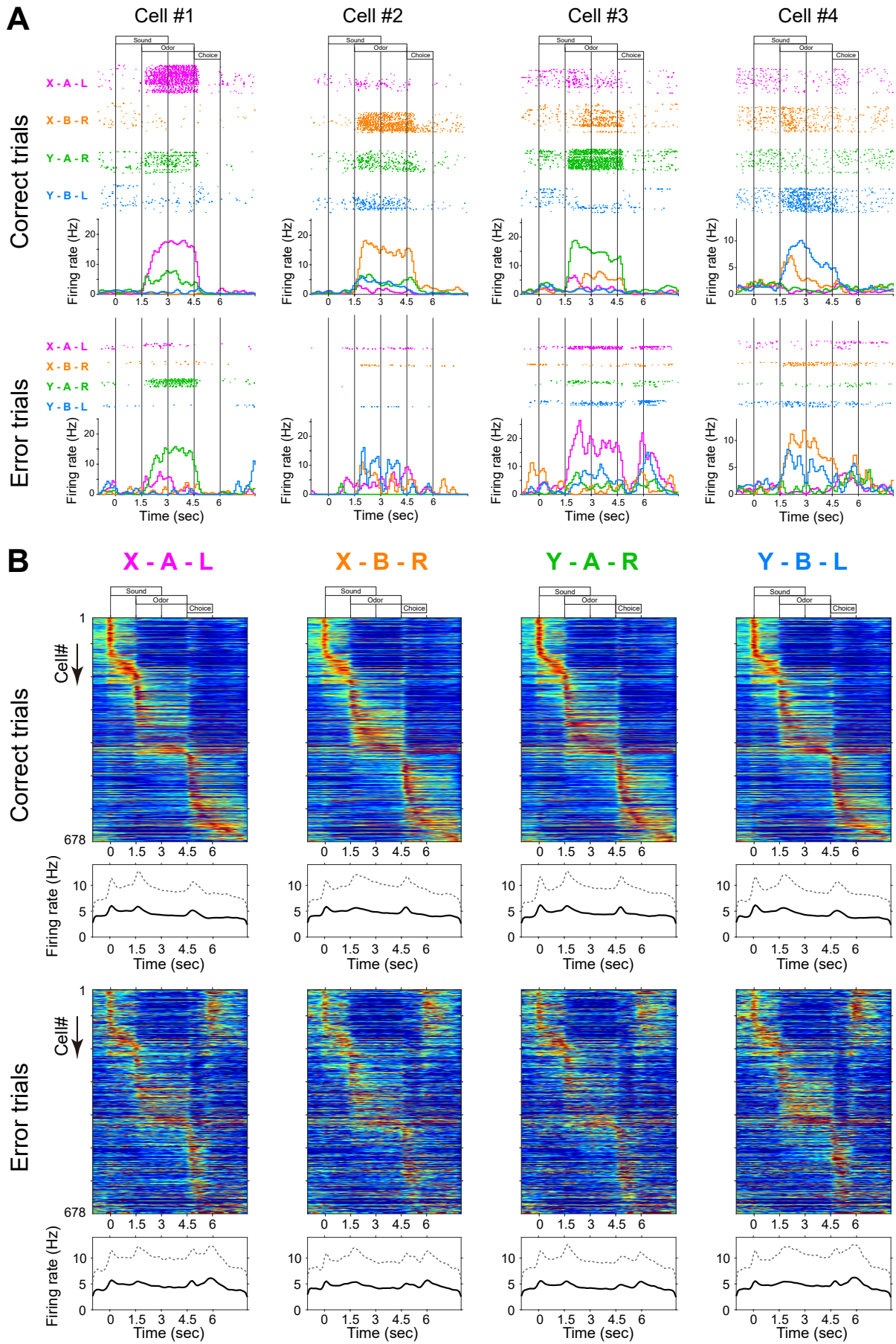


Figure S5 (A-B). Population vector analysis in correct and error trials, related to Figure 3.

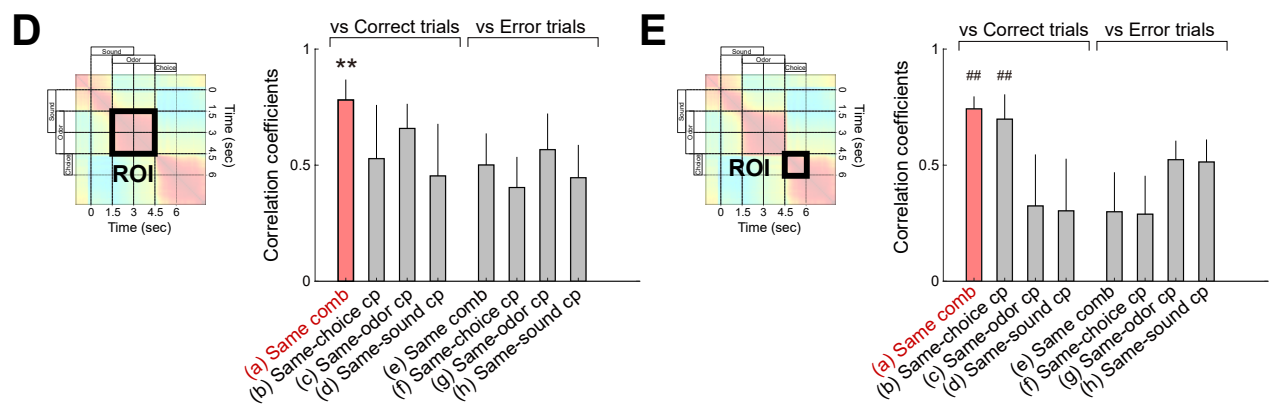
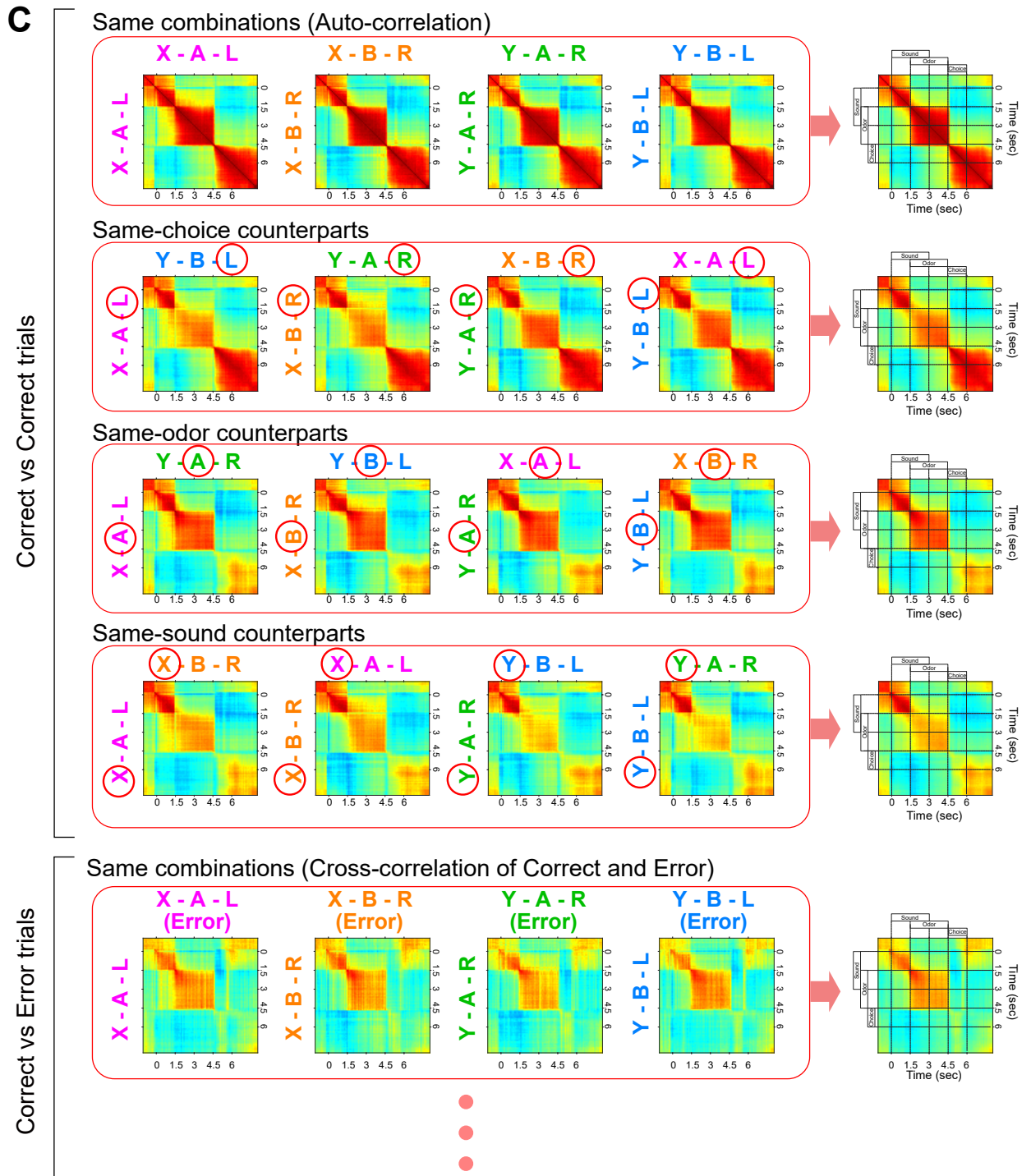


Figure S5 (C-E). Population vector analysis in correct and error trials, related to Figure 3.

Figure S5. Population vector analysis in correct and error trials, related to Figure 3.

(A) Firing patterns of four representative neurons in correct (*top*) and error (*bottom*) trials. The same neurons shown in Figure 3A were displayed.

(B) Population vectors of pyramidal neurons in each combination condition in correct (*top*) and error trials (*bottom*). Sessions that contained at least 2 error trials in each combination condition were selected in this analysis (n=678 units in 30 sessions). Overall mean firing rates of all neurons in each combination condition in correct and error trials are also shown (Mean+SD).

(C) How to compute the auto-correlations and cross-correlations of population vectors. (1) Same combinations. Auto-correlation of population vectors in each combination condition in correct trials (see, Fig S5B) was computed. Then, the average of auto-correlations of four conditions were calculated. (2) Same-choice counterparts. Cross-correlations between two combination conditions which have same choice, i.e., XAL vs YBL, XBR vs YAR, YBL vs XAL, YAR vs XBR, were computed. Then, the average of these were computed. (3) Same-odor counterparts. Cross-correlations between two combination conditions which have same odor, i.e., XAL vs YAR, XBR vs YBL, YAR vs XAL, YBL vs XBR, were computed. (4) Same-sound counterparts. Cross-correlations between two combination conditions which have same sound, i.e., XAL vs XBR, XBR vs XAL, YAR vs YBL, YBL vs YAR, were computed. (5) Same combinations (Correct vs Error). Cross-correlations between population vectors of correct and error trials in the same combination conditions, i.e., XAL(Correct) vs XAL(Error), XBR(Correct) vs XBR(Error), YAR(Correct) vs YAR(Error), YBL(Correct) vs YBL(Error), were computed. Other types of cross-correlations of population vectors of correct and error trials were computed similarly.

(D) Mean correlation coefficients in the area of odor presentation periods (1.5-4.5 sec; shown as ROI in inset) of auto- and cross-correlations of population vectors. In this analysis (D and E), population vectors and their correlations were computed in each session. (n=30 sessions; Sessions which had at least 2 error trials in each combination condition were selected).

(E) Mean correlation coefficients in the area of choice periods (4.5-6 sec; shown as ROI in inset).

**P<0.01 vs b, d, e, f, g and h; ##P<0.01 vs c, d, e, f, g and h; ANOVA and post-hoc Tukey-Kramer test.

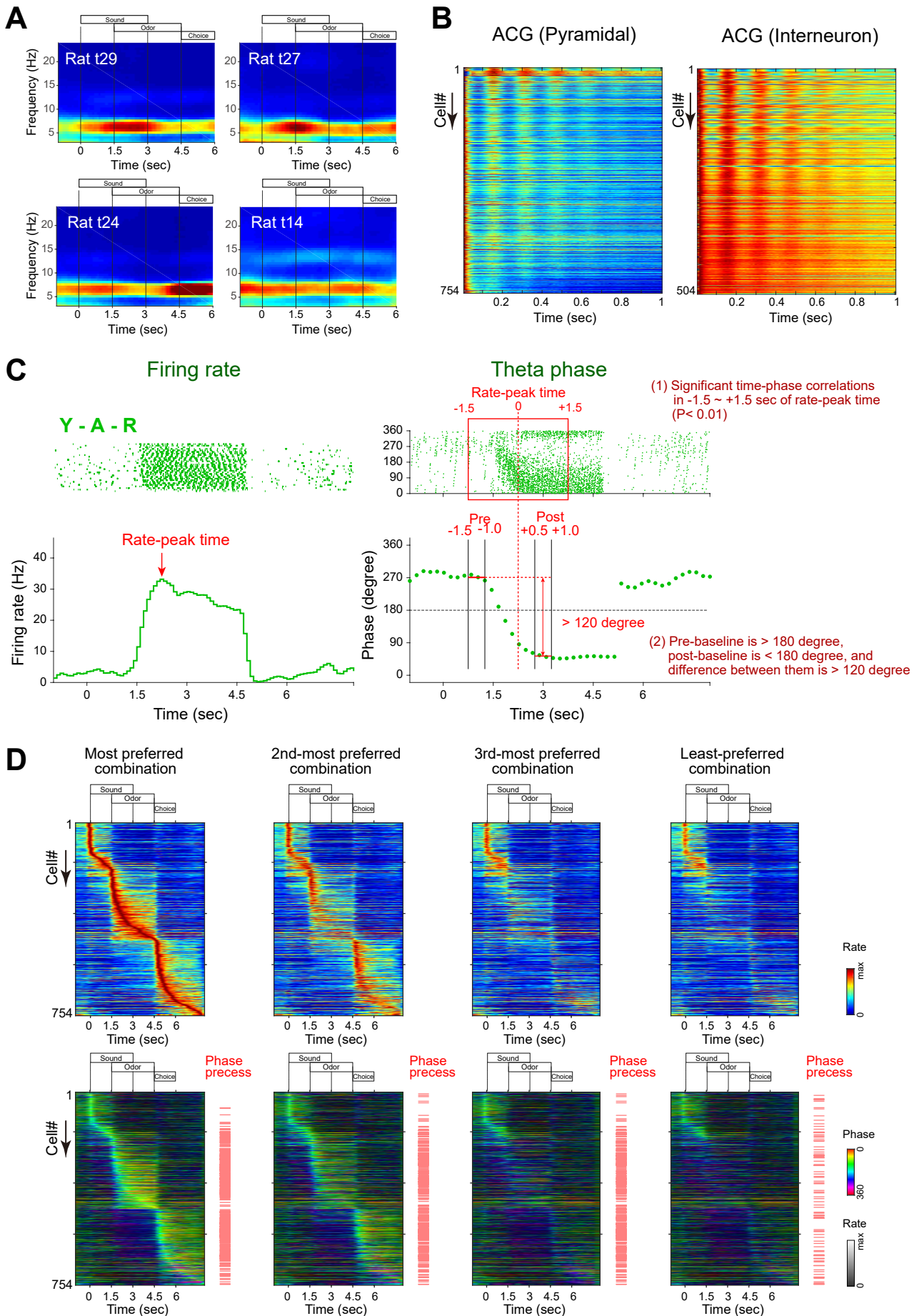


Figure S6 (A-D). Theta modulations of LFPs and units during the task, related to Figure 4.

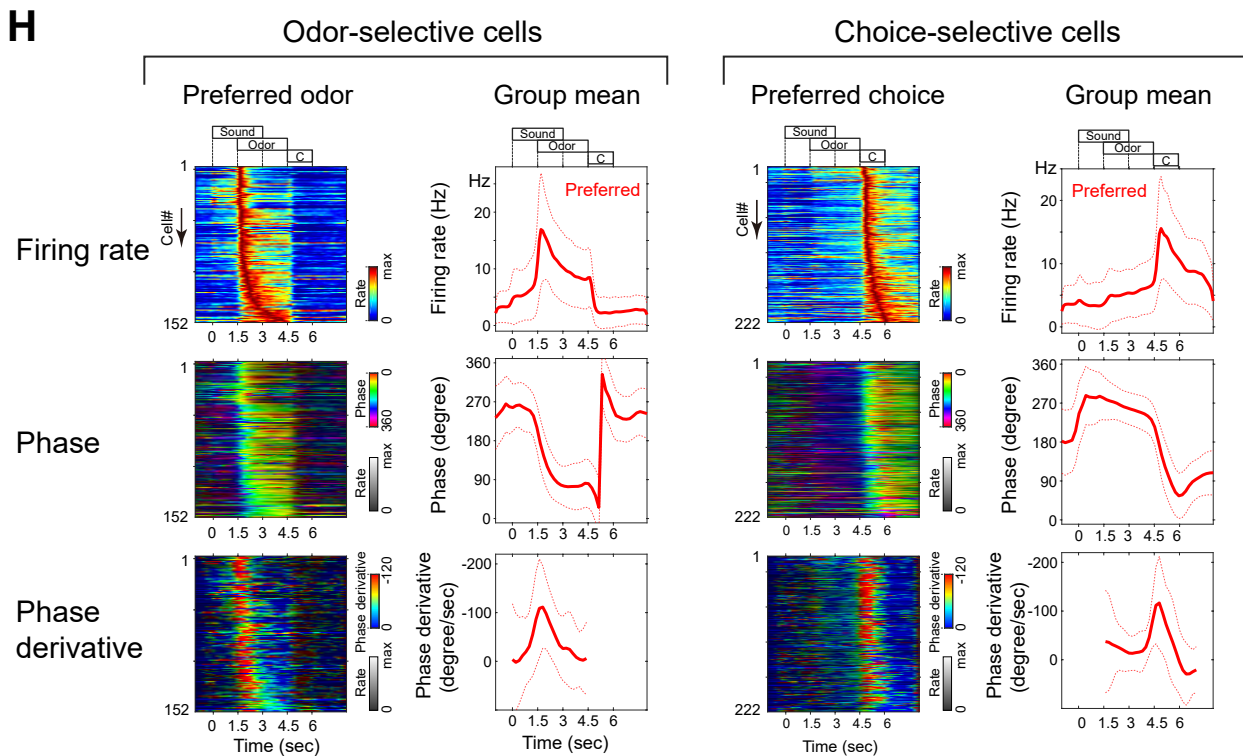


Figure S6. Theta modulations of LFPs and units during the task, related to Figure 4.

(A) Representative time-resolved power spectrum of LFP in CA1 during a single session in each rat.

(B) Auto-correlograms (ACG) of all single pyramidal neurons and interneurons during the task trials ($n=754$ units for pyramidal cells; $n=504$ units for interneurons).

(C) Criteria of theta phase precession. The presence of theta phase precession was assessed in each neuron in each combination condition, with using following three criteria; (i) there was a significant linear-circular correlation ($P < 0.01$; Berens 2009) between time and theta phases, in the period between -1.5 sec to 1.5 sec of the time of the peak firing rate, (ii) the phases crossed 180° (troughs of theta) in the period between -1.5 sec to 1.5 sec of peak time, and (iii) the phase shift was more than 120° .

(D) Firing rates and theta phases of all single pyramidal neurons. *Top*, normalized firing rates of odor-selective neurons in each combination condition. These are the same panels of Figure 3B. *Bottom*, corresponding theta phases. Hue represents theta phases (0 - 360 degree), and brightness represents normalized firing rates in each neuron. Red lines indicate the presence of theta phase precession in our criteria. See also, Figure S7.

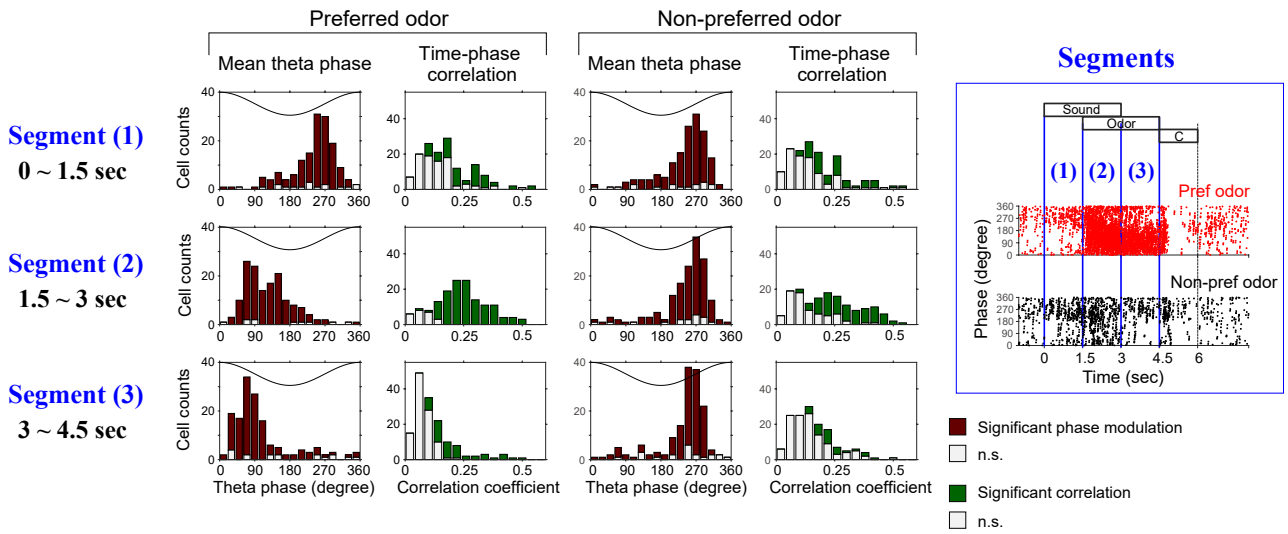
(E) Enlarged panel of Figure 4B.

(F) Enlarged panel of Figure 4D.

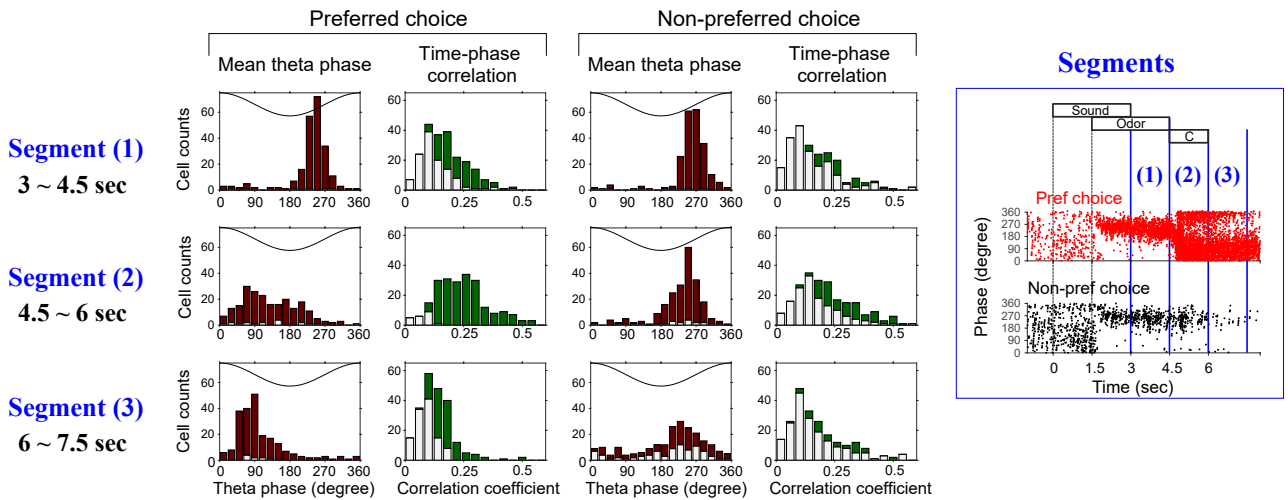
(G) Enlarged panel of Figure 4F.

(H) Slopes of phase precession in odor-/choice-selective neurons (see, Figure 4). The slope of phase precession was computed as the derivative of the phase plot in each neuron. Majority of the neurons showed transient increase of phase slope only around the onset of the preferred events. The same sets of neurons used in Figure 4B and D are shown here. Mean (Thick lines) \pm SD (dotted lines).

A Odor-selective cells



B Choice-selective cells



C Combination-selective cells

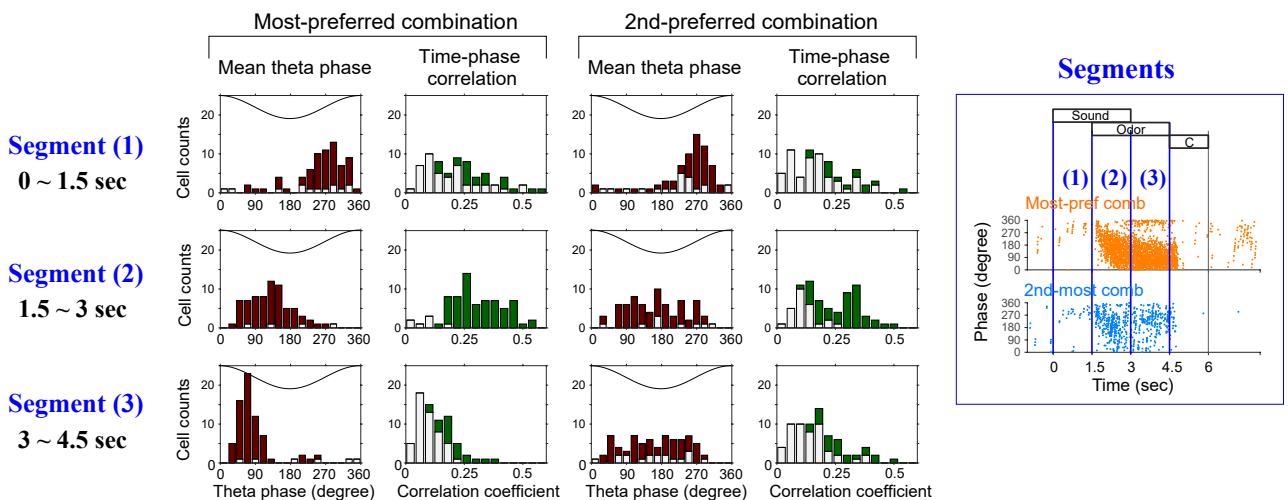


Figure S7. Phase locking and phase precession in different time periods, related to Figure 4.

Figure S7. Phase locking and phase precession in different time periods, related to Figure 4.

(A) Phase locking and phase precession of odor-selective neuron were quantified in the time periods before odor presentation (Segment 1: 0-1.5sec), during early half of odor presentation (Segment 2: 1.5-3 sec), and during late half of the odor presentation (Segment 3: 3-4.5 sec), in preferred (*left block*) and non-preferred (*right block*) trials.

(*Left column in each block*) Histogram of phase preferences of single neurons in each time segments. Dark red indicates neurons with significant phase modulation by theta oscillation ($P < 0.01$; Rayleigh test)

(*Right column in each block*) Histogram of coefficients of time-phase correlations of single neurons in each time segments. Dark green indicates neurons with significant time-phase correlations ($P < 0.01$; Berens 2009)

(*Right inset*) Segments 1, 2 and 3 are indicated on theta phase plots of an example odor-selective cell.

The same set of neurons in Figure 4B were analyzed here ($n=152$ units).

(B) Phase locking and phase precessions of choice-selective neuron were quantified in the time periods before choice (Segment 1: 3-4.5sec), during choice (Segment 2: 4.5-6 sec), and after choice (Segment 3: 6-7.5 sec), in preferred (*left block*) and non-preferred (*right block*) trials. The same set of neurons in Figure 4D were analyzed here ($n=222$ units).

(B) Phase locking and phase precessions of combination-selective neuron were quantified in the time periods before odor presentation (Segment 1: 0-1.5sec), during early half of odor presentation (Segment 2: 1.5-3 sec), and during late half of the odor presentation (Segment 3: 3-4.5 sec), in most-preferred (*left block*) and second-most-preferred (*right block*) trials. The same set of neurons in Figure 4F were analyzed here ($n=72$ units).

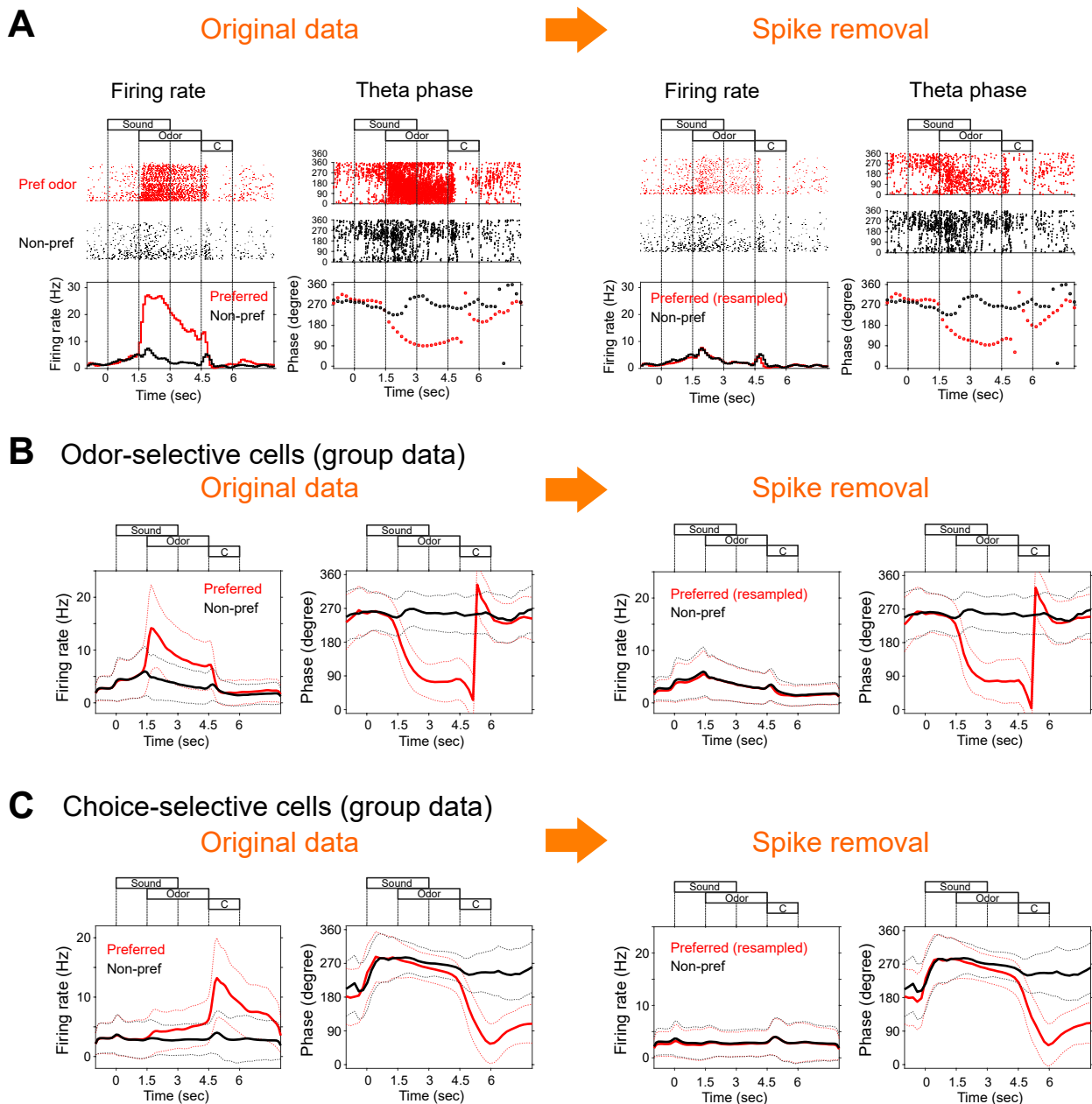


Figure S8. Differences of phase precession between preferred and non-preferred trials were not due to detectability, related to Figure 4.

Theta phase precession might not be detected when firing rates were very low in our criteria. To rule out the possibility that the results of differences of phase precession between preferred and non-preferred trials were due to this detectability problem, analysis to test the detectability of phase precession was conducted. In this analysis, we equalized the firing rates in preferred and non-preferred trials, by randomly removing spikes from preferred trials (A). Even after equalization of the firing rates between preferred and non-preferred trials, we still observed the robust phase precession in preferred trials, as shown in (B) and (C). Thus, the phase differences between preferred and non-preferred events were not because of the differences of the detectability due to firing rates. Here, the same datasets of Figure 4B and D were used.

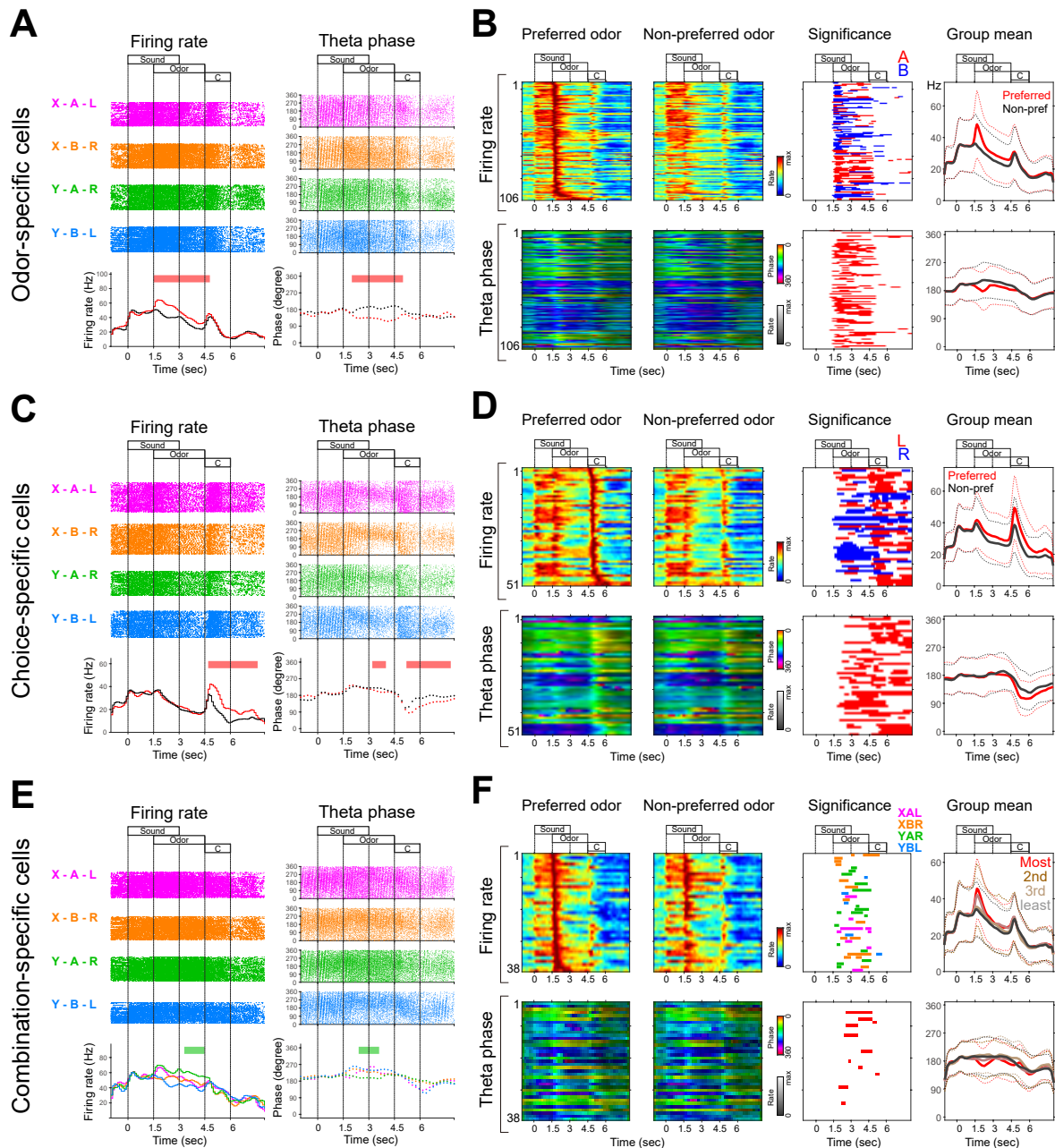


Figure S9. Temporal and rate coding of single interneurons during the cue-combination task, related to Figure 4.

(A) Firing rates and theta phases of a representative odor-selective interneuron. *Left*, raster plots and PSTHs. *Right top*, theta phase plot as a function of time from stimulus onsets. Each dot represents action potential. *Right bottom*, mean theta phases as a function of time during Odor-A (blue) and B (red) trials. Lines above PSTHs and phase plots represent segments with significantly higher firing rates and with significant phase differences, respectively ($P < 0.05$; see Figure 4).

(B) Firing rates and theta phases of odor-selective interneurons ($n=106$ units). *Top*, firing rates of odor-selective neurons during preferred- and non-preferred-odor trials. Third column shows segments with significantly higher discharge rates in Odor-A (red) or Odor-B (blue) trials ($P < 0.05$; Permutation test). Right column shows mean firing rates (thick lines) \pm SD (dotted lines). *Bottom*, theta phases as a function of time during preferred- and non-preferred-odor trials. Hue represents theta phases (0-360 degree), and brightness represents normalized firing rates in each neuron. Third column shows segments with significantly different phases in different odor trials. ($P < 0.05$ for one side; Permutation test). Right column shows mean phases \pm SD.

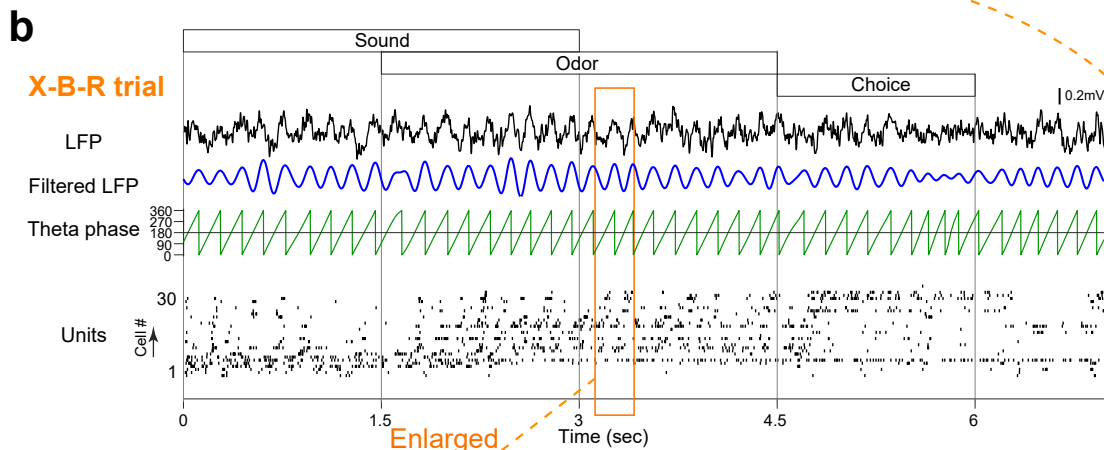
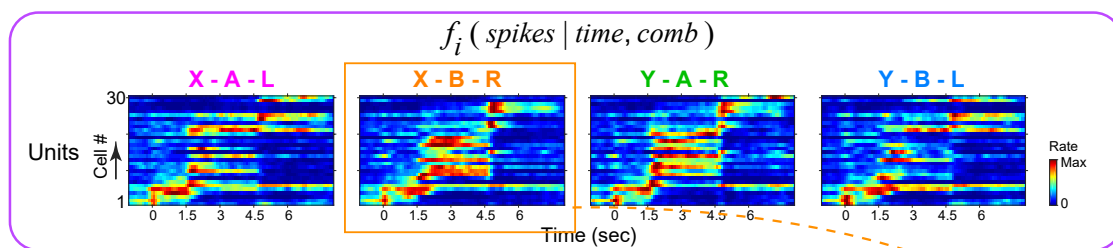
(C) Firing rates and theta phases of a representative choice-selective interneuron.

(D) Firing rates and theta phases of choice-selective interneurons ($n=51$ units).

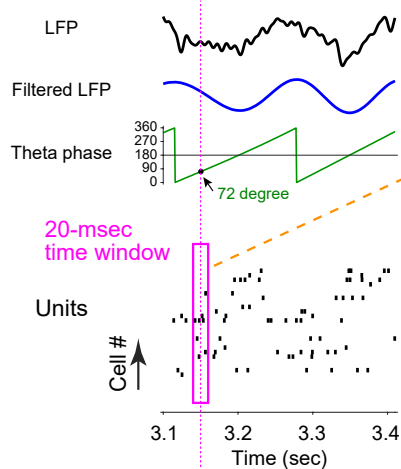
(E) Firing rates and theta phases of a representative combination-selective interneuron.

(F) Firing rates and theta phases of combination-selective interneurons ($n=38$ units).

A a Prior probabilities were estimated from the PSTHs of cells in each combination.

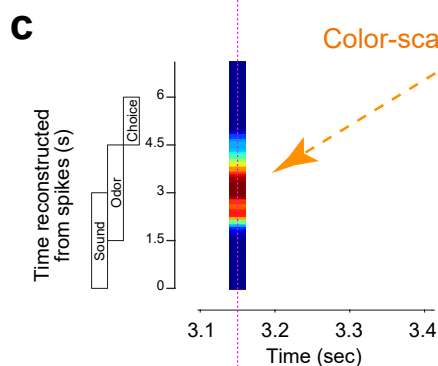
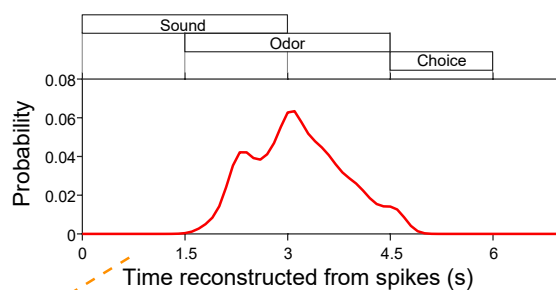


Move a window with 5ms step



Perform Bayesian decoding of time information using spikes within this 20-msec time window

$$P(\text{time} | \text{spikes}, \text{comb})$$



Sampled time = 3.15 sec

Theta phase = 72 degree

Aligned with sampled time
→ Fig 6A bottom

Aligned with theta phase
→ Fig 6B, C & D

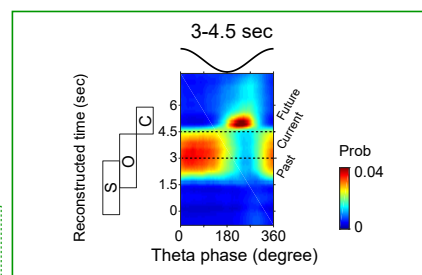
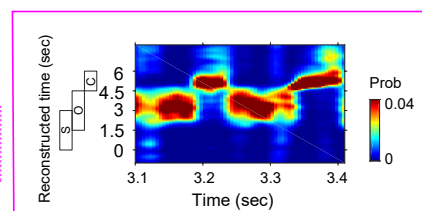
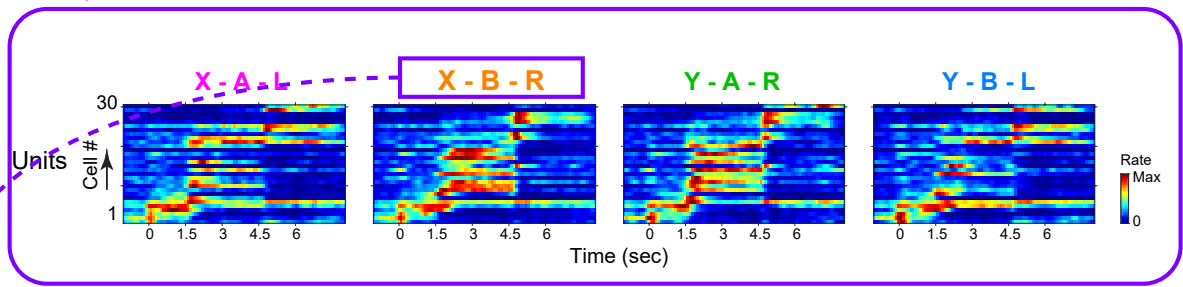
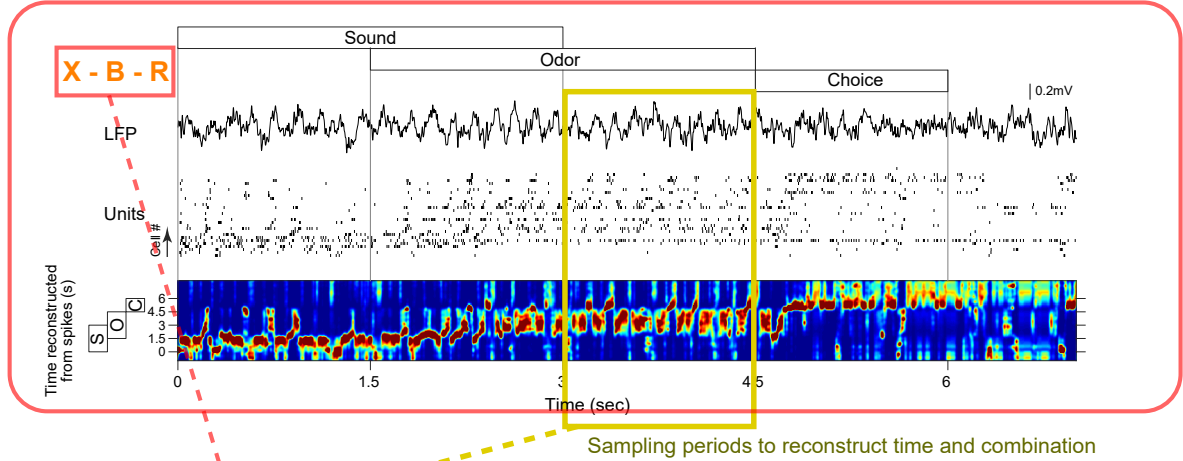


Figure S10 (Aa-c). Procedures of Bayesian decoding, related to Figure 6.

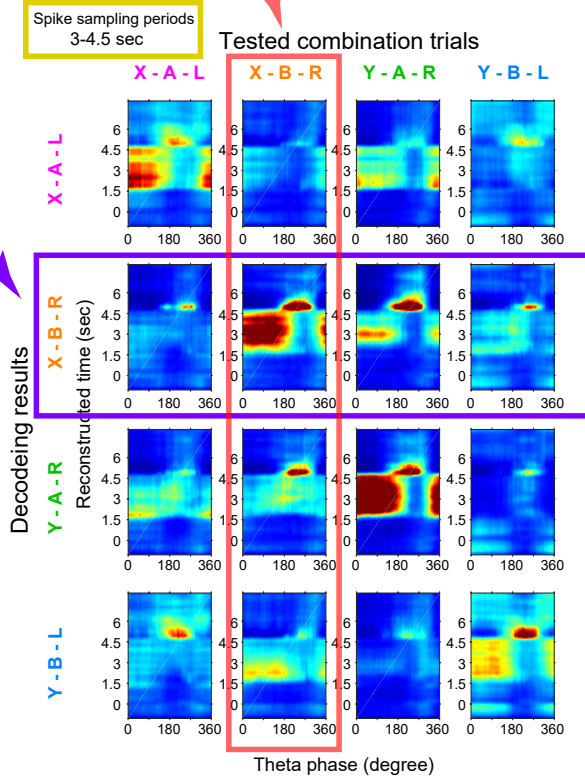
B a Prior probabilities were estimated from the PSTHs of cells in each combination.



b Posterior probabilities were estimated in each time bin in each trial in each combination.



c Correct trials



Error trials

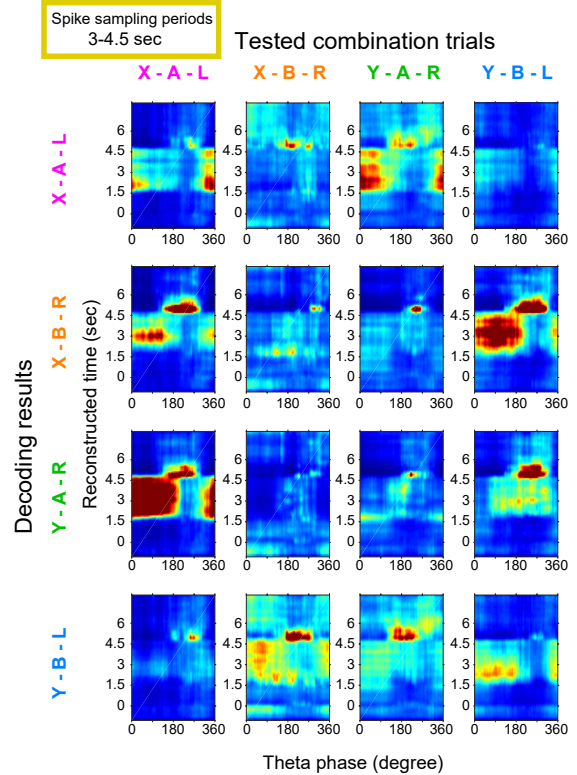


Figure S10 (Ba-c). Procedures of Bayesian decoding, related to Figure 6.

Figure S10. Procedures of Bayesian decoding, related Figure 6.

(See also, Figure 6; STAR Methods; Feng et al., 2015; Davidson et al., 2009)

(A) Procedures of reconstruction of time information.

(Aa) First, PSTHs of single neurons in each combination condition in a single session were estimated. This is expressed as $f_i(time, comb)$, where i is the index of the neurons.

(Ab) In each trial, Bayes decoding was performed every 5-ms time step. At each time point, we set 20-ms time window. Spike counts of each neuron, n_i , were estimated in the 20-ms time window. Then, time information was reconstructed from neuronal activities in this 20-ms time window, as using the following equation

$$P(time|spikes, comb) = C \cdot P(time|comb) \left(\prod_{i=1}^N \frac{(\tau f_i(time|comb))^{n_i}}{n_i!} \right) \exp \left(-\tau \sum_{i=1}^N f_i(time|comb) \right)$$

where τ is the time window of sampling spike trains (i.e., 20 ms), and C is a normalization factor (Methods). Here (Figure 6A-C), we only decoded time formation, so combination information was conditioned.

At each sampling time point, instantaneous theta phase was also calculated.

The plot of Figure 6A was made by aligning the decoded time information with time stamps of sampling times.

The plots of Figure 6B & C were made by aligning the decoded time information with concurrent theta phases.

(B) Procedures of reconstruction of time and combination information.

(Ba) PSTHs of single neurons in each combination condition in a single session were estimated, as describes above.

(Bb) In each trial, Bayes decoding was performed every 5-ms time step, as described above. Then, information of time and combination was reconstructed from neuronal activities in this 20-ms time window, as using the following equation

$$P(time, comb|spikes) = C \cdot P(time, comb) \left(\prod_{i=1}^N \frac{(\tau f_i(time, comb))^{n_i}}{n_i!} \right) \exp \left(-\tau \sum_{i=1}^N f_i(time, comb) \right)$$

Here (Figure 6D-F), we decoded both time and combination formation.

(Bc) Probability densities of the time and combination information as a functions of theta phase were estimated from spikes (sampled in time segment 3~4.5 sec) in each combination condition, in correctly answered (left) and error (right) trials in each session. This is a representative result from a single session which is the same one in Figure 6D.

The following table explains the pairs of the prior and the sampled combination patterns.

| | | Tested | | | |
|-------|-----|--------|-----|-----|-----|
| | | XAL | XBR | YAR | YBL |
| Prior | XAL | 1 | 4 | 3 | 2 |
| | XBR | 4 | 1 | 2 | 3 |
| | YAR | 3 | 2 | 1 | 4 |
| | YBL | 2 | 3 | 4 | 1 |

1. 'Same combinations'
2. 'Same-choice counterparts'
3. 'Same-odor counterparts'
4. 'Same-sound counterparts'

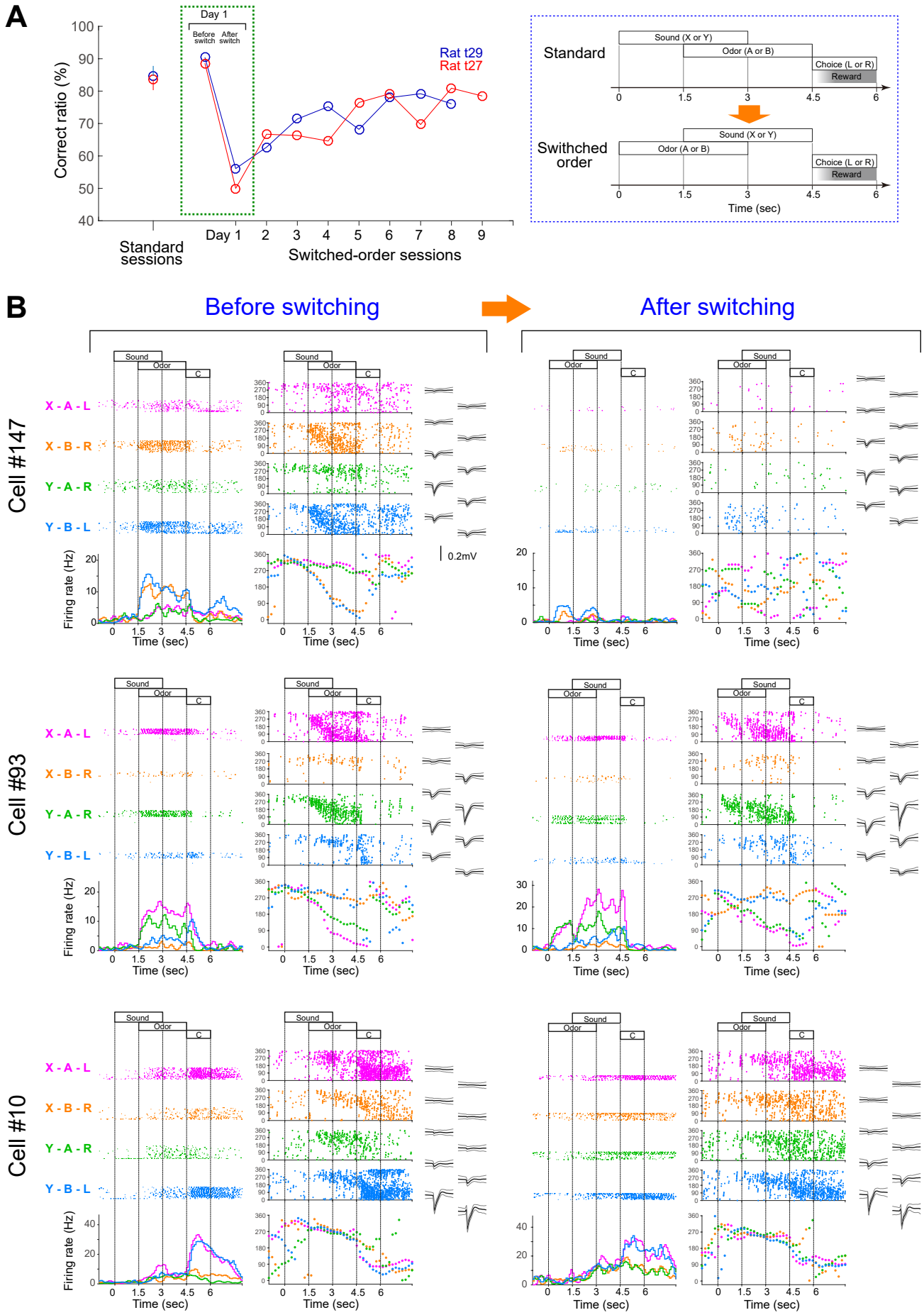


Figure S11 (A-B). Partial remapping of neuronal activities in the first day of order switching, related to Figure 7.

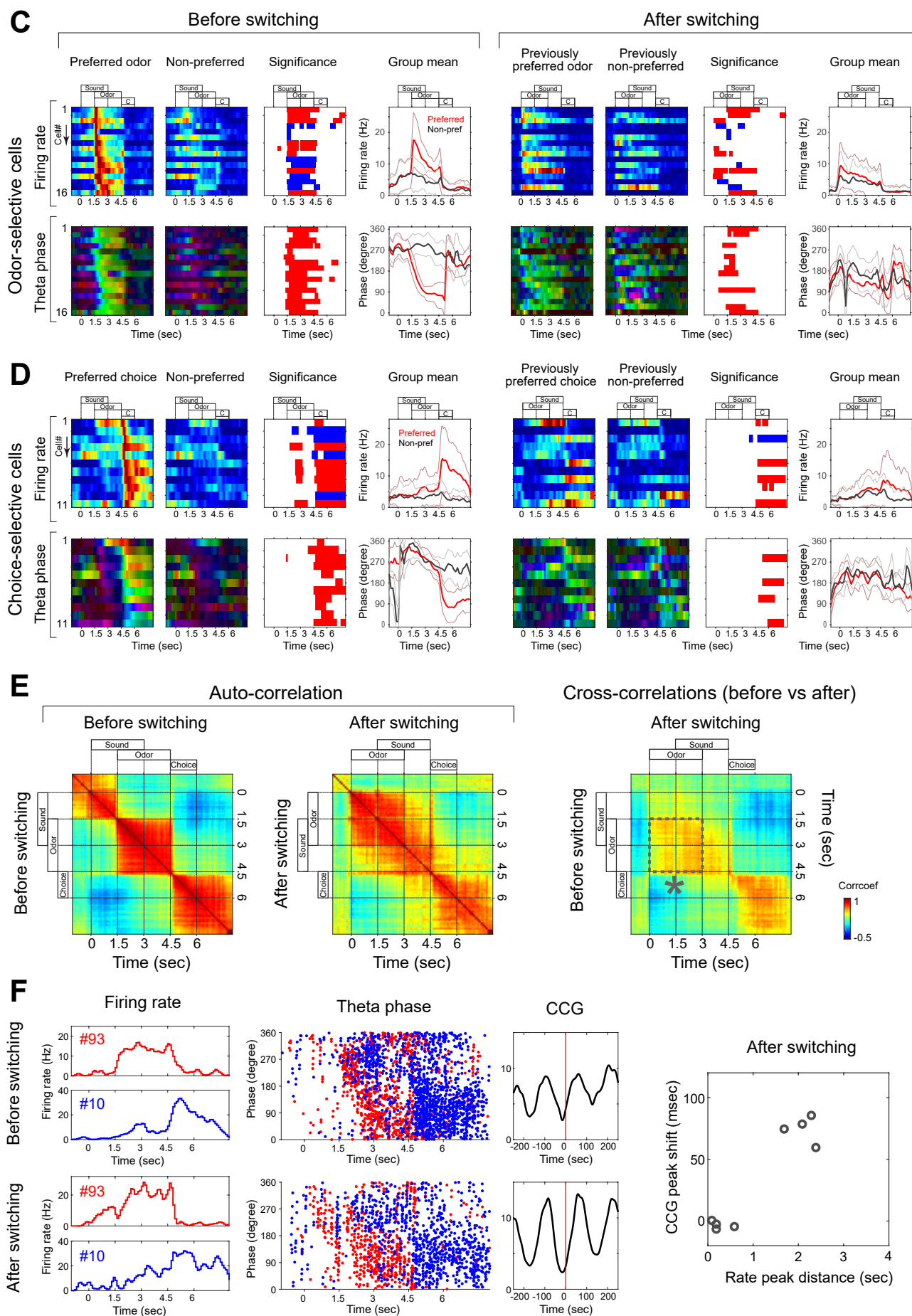


Figure S11 (C-F). Partial remapping of neuronal activities in the first day of order switching, related to Figure 7.

Figure S11. Partial remapping of neuronal activities in the first day of order switching, related to Figure 7.

(A) Learning curves of the cue-combination task after switching the order of cue presentations. In the first day of the order-switching, the recoding experiments were performed continuously in a single session without break (total 80 min; 0~30 min for trials 'before switching', 30~80min for 'after switching').

(B) Firing rates and theta phases of three representative neurons before and after switching the orders of stimuli in the first day. Cell#147 displayed huge decrease of the firing rates after switching the order, whereas Cell#93 and Cell#10 almost preserved their rates and preferences for stimuli or choices. The waveforms of each neuron before and after order switching are also shown. These cells were recorded from the same rat.

To validate the unit stability, we computed the Mahalanobis distances of spike clusters in 30-dimensional space (10 channels x 3 features) for each identified units. The Mahalanobis distances of the spike clusters before switching, after switching and overall (before+after) were 28.630 ± 2.533 , 28.628 ± 2.533 , and 28.634 ± 2.533 , respectively (mean \pm SD, n=66 units), indicating the units were stable during the sessions.

(C) Firing rates and theta phases of odor-selective pyramidal neurons before (*left*) and after (*right*) switching the order in the first day (n=16 units). *Top*, firing rates of odor-selective neurons during preferred- and non-preferred-odor trials. Third column shows segments with significantly higher discharge rates in Odor-A (red) or Odor-B (blue) trials ($P < 0.05$; Permutation test). Fourth column shows mean firing rates (thick lines) \pm SD (dotted lines). *Bottom*, theta phases as a function of time during preferred- and non-preferred-odor trials. Hue represents theta phases (0-360 degree), and brightness represents normalized firing rates in each neuron. Third column shows segments with significantly different phases in different odor trials. ($P < 0.05$ for one side; Permutation test). Forth column shows mean phases \pm SD. Color-coded rate map of cells after switching was normalized by the maximum firing rate before switching for each cell.

(D) Firing rates and theta phases of odor-selective neurons before (*left*) and after (*right*) switching the order in the first day (n=11 units).

(E) Auto-correlations and cross-correlation of population vectors of neuronal activities before and after order switching (n=66 units of pyramidal neurons). Note that relatively high correlation was observed in the area of odor-representing periods for before and after switching (shown in asterisk) in the cross-correlation.

(F) Pairwise analysis of temporal compression of spike sequence before and after switching. In the first day of the switching, 4 of odor-selective neurons (25.0%) and 4 of choice-selective neurons (36.3%) preserved their temporal and rate coding for event selectivity. (The criteria was that (i) the event preferences after switching were same as those before switching, (ii) there were significant phase differences between preferred and non-preferred events both before and after switching, (iii) the maximum firing rates after switching was no less than half of those of before switching.) We applied pairwise analysis for these 8 of feature-preserved neurons. *Left*, cross-correlations of a representative pair of neurons (Cell#93 and #10; also shown in Fig S14B) during the combination X-A-L trials before (*top*) and after (*bottom*) switching. *Right*, pairwise analysis of temporal compression of spike sequence after switching (n=8 pairs; $R^2 = 0.857$; $P < 0.01$).